
# Thermogravimetric insight in the reduction of xCuO – (1-x)MoO3 oxide system ($0.1 \leq x \leq 0.9$) by hydrogen

Dijana Jelić, Saša Zeljković, Dragana Jugović, Slavko Mentus

PII: S0263-4368(21)00012-3

DOI: https://doi.org/10.1016/j.ijrmhm.2021.105480

Reference: RMHM 105480

To appear in: *International Journal of Refractory Metals and Hard Materials*

Received date: 13 December 2020

Revised date: 10 January 2021

Accepted date: 10 January 2021

Please cite this article as: D. Jelić, S. Zeljković, D. Jugović, et al., Thermogravimetric insight in the reduction of xCuO – (1-x)MoO3 oxide system ($0.1 \leq x \leq 0.9$) by hydrogen, *International Journal of Refractory Metals and Hard Materials* (2019), https://doi.org/10.1016/j.ijrmhm.2021.105480

# Thermogravimetric insight in the reduction of xCuO – (1-x)$MoO_3$ oxide system ($0.1 \leq x \leq 0.9$) by hydrogen

Dijana Jelić[1], Saša Zeljković[1], Dragana Jugović[2] and Slavko Mentus[3,4]

[1]Department of Chemistry, Faculty of Natural Sciences and Mathematics, University of Banja Luka, dr Mladena Stojanovića 2, 78 000 Banja Luka, Bosnia and Herzegovina

[2]Institute of Technical Sciences of Serbian Academy of Sciences and Arts, Knez Mihajlova 35, 11000 Belgrade, Serbia

[3]Faculty of Physical Chemistry, University of Belgrade, Studentski trg 12, Belgrade 11000, Serbia

[4]Serbian Academy of Sciences and Arts, Knez Mihajlova 35, Belgrade 11000, Serbia

Abstract

The oxide mixtures xCuO-(1-x) $MoO_3$ were synthesized by gel-combustion procedure. The existence of phase mixture CuO + $Cu_3Mo_2O_9$ and $MoO_3$ + $CuMoO_4$ in CuO-rich and $MoO_3$-rich composition region, respectively, were evidenced. The constant heating rate thermogravimetry in hydrogen atmosphere revealed that the reduction reactions proceed within the two clearly separated temperature regions. On the basis of mass changes, the mechanism of reduction processes was discussed. The measurements revealed considerable inhibition of CuO reduction by $MoO_3$, and huge acceleration of $MoO_3 \rightarrow MoO_2$ reduction step by copper. The particularities found in this system were commented in relation to our similar studies in NiO-$MoO_3$ and CuO-$WO_3$ systems. For particular composition, x = 0.5, existing preferably in form of a-$CuMoO_4$, kinetic parameters of reduction were determined. The composition of oxide mixture influenced the particle size and morphology of resulting metallic Cu-Mo composites.

**Key words:** copper oxide; Cu-Mo composites; hydrogen; molybdenum oxide; thermogravimetry

## 1. INTRODUCTION:

The mixtures of copper and molybdenum oxides have been the subjects of many published studies. According to the phase diagram published in 1979 [1], at the mole ratios CuO : $MoO_3$ of 1:1 and 3:2, the components may build up stable solid compounds with the formulae $CuMoO_4$ and $Cu_3Mo_2O_9$. Both CuO and CuO-$MoO_3$ mixtures at particular molar ratios are used as heterogeneous catalysts for many redox reactions, like carbon monoxide oxidation [2], synthesis of methanol [3], and atmosphere protection from toluene vapor [4]. Wang et al. [5] showed that CuO (5 wt%) - $MoO_3$ (10 wt%) mixture on the $Al_2O_3$ support exhibit high activity for the destructive oxidation of $(CH_3)_2S_2$. The formation of complex oxide compounds was considered as a factor of catalytic activity. For instance, Soltys et al. [6] published that the conversion of simple CuO-$MoO_3$ mixtures to the compounds $Cu_{4-x}Mo_3O_{12}$ and $Cu_6Mo_5O_{18}$ displays notable impact on the active state of these catalysts [6]. Shaheen et al [7] synthesized three CuO-$MoO_3$ mixtures by heating thermodegradable solids under TG/DTA control, and investigated their catalytic activity toward hydrogen peroxide decomposition in terms of formation of $CuMoO_4$. Recently crystalline flower-like $Cu_3Mo_2O_9$ was studied as an anode material of lithium-ion batteries [8, 9]

The CuO-$MoO_3$ oxide systems were considered often as a way to produce powdery Cu-Mo composites by means of various reduction agents. Compacted Cu-Mo composites of particular mole ratio of constituents are suitable for heavy duty current switchers and welding electrodes. The uniformity of metallic particle radii of composites depends on the homogeneity of starting oxide mixture. To obtain suitable oxide mixtures, apart of Pechini method [10],

gelatinization of oxides with acrylamide [11], citrate gel-combustion [12,13,14], low temperature coprecipitation [15] were considered in the literature. Song et al. [11], reduced acrylamide-gelatinized CuO-MoO3 solution by hydrogen to obtain powdery metallic Mo-15 wt.%Cu composite. Zhao et al [12] synthesized CuO-$MoO_3$ mixture by citrate gel-combustion method, and transformed it into powdery Mo-30wt% Cu composite by reduction with hydrogen. Somewhat complicated way to obtain Cu-Mo composite, namely, the reduction of CuO-$MoO_3$ mixture by carbon and magnesium, was attempted by Kirakosyan et al [16]. Yazdi et al. [17] attempted to obtain Cu-Mo composite by ball milling of CuO-$MoO_3$/C mixtures, where carbon served as reduction agent. Sun et al [18] homogenized the mixture of CuO and $MoO_3$ by ball milling and transformed it into nanodispersed core/shell structured Cu-Mo composite by reduction in hydrogen atmosphere. Recently, Ji et al. prepared ultra-fine Mo-10 wt% Cu composites by a two-step process, first via carbothermal reduction, and subsequently by reduction in gaseous hydrogen. [19]

The available literature data show that both CuO and $MoO_3$ and their compounds may be reduced to metallic state if heated in hydrogen atmosphere. Pure CuO may be easily reduced at relatively low temperatures, 150-250 $^{o}$C [20-25]. Under particular conditions, all possible intermediate states ($CuO \rightarrow Cu_4O_3 \rightarrow Cu_2O \rightarrow Cu$) were observed [21], however, in most cases the number of observed reaction steps was limited to either single one ($CuO \rightarrow Cu$) [20, 22-25] or to two ones ($CuO \rightarrow Cu_2O \rightarrow Cu$) [22]. For instance, Kim et al.[22], revealed that the reduction is single-step process if hydrogen flow rate is higher than 15 mL min$^{-1}$, and two-step process if gas flow rate is less than 1 mL min$^{-1}$. Vong et al. [23 ] and Rodriguez et al. [24,25] studying the CuO reduction by X-ray diffraction method concluded that the reduction reaction proceeds directly to the metallic state, without any intermediates.

The kinetics and mechanism of reduction of $MoO_3$ are widely investigated, mostly under hydrogen flow [26-32, 34, 35], and somewhere in CO-$CO_2$ atmosphere [33]. Two main steps, $MoO_3 \rightarrow MoO_2$ and $MoO_2 \rightarrow Mo$, are found to be kinetically well separated, so some authors studied only the first step [32,34] while some others studied only the second step [34,35]. In CO-$CO_2$ atmosphere several reduction intermediates of descending valence were observed, and moreover, formation of $MoC_2$ was revealed [33]

Since in the CuO-$MoO_3$ oxide system the interaction between the components may lead to the formation of complex oxides –various forms of copper molybdate [1], one may expect more complicated reduction mechanism in this oxide system in comparison to the reduction mechanism of pure ingredients. This topics is important from both theoretical and practical aspects, as one may reasonably expect that the reaction kinetics and mechanism influences the morphology and homogeneity of resulting Cu-Mo composite. In spite of the fact that many studies dedicated to the synthesis of Cu-Mo composite by reduction of CuO-$MoO_3$ mixtures were published in scientific journals, very rarely these studies were focused on the kinetics and mechanism of the reduction processes, and moreover, very limited number of mole ratios were considered, focused at the compositions most suitable for production of particular Cu-Mo composites, preferably in the middle region of molar ratios. For instance, Zhao et al [12] in the mixture targeted to give Mo-30 wt% Cu composite, by the temperature programmed reduction (TPR) procedure, found the three maxima of $H_2$ consumption, at 250, 380 and 620 $^oC$, which were attributed to $CuMoO_4$ reduction and to two steps of $MoO_3$ reduction, respectively. Kirakosyan et al. [16] subjected the $CuMoO_4$/C mixture to the reduction, where carbon served as the reduction agent. Using thermogravimetry and X-ray diffractometry as reaction controlling methods, they found that $CuO \rightarrow Cu_2O$ reduction proceeds up to 500 $^oC$ and simultaneous

$Cu_2O \rightarrow Cu$ and $MoO_3 \rightarrow MoO_2$ reduction proceeds up to 700 $^oC$. Although these studies are helpful, they are insufficient to predict successfully the reduction kinetics and mechanism for $CuO\text{-}MoO_3$ oxide system in an expanded range of molar ratios.

This lack in knowledge about this important system incited us to study the reduction of $xCuO:(1\text{-}x)MoO_3$ oxide mixtures in broad range of molar ratios, by systematic variation of mole ratios in a range $0.1 < x < 0.9$, using constant heating rate thermogravimetry as a sensitive method to trace kinetics and mechanism of reduction process. Hydrogen was used as a reduction agent since, according to our previous experience with CuO and $CuO\text{-}WO_3$ system [13, 20] it enables simpler reduction mechanisms than either $CO/CO_2$ mixture [33] or solid reduction agents (C, Mg) [16]. This study revealed that the interactions between the ingredients induced huge changes in kinetics of mixtures reduction in comparison to pure ingredients. Formerly, some of us published analogous investigations of the system $NiO\text{-}MoO_3$ [36], and the observed differences were commented. For particular composition, 0.5 CuO - 0.5 $MoO_3$, which exist preferably as the compound $\alpha\text{-}CuMoO_4$, the reduction was analysed from the scope of kinetic point of view, employing isoconversional (expanded Friedman, modified Kissinger and Flyn-Wall-Ozawa) and model-fitting (nucleation and growth) approach under non-isothermal conditions. The mean particle size of Cu-Mo composites were observed by scanning electron microscopy, and their consequences on reduction kinetics were considered.

## 2. EXPERIMENTAL

**Materials and methods:** Formerly, citrate gel-combustion method, was proved by us to enable good control of stoichiometry, good chemical homogeneity of obtained gel and good chemical homogeneity of the product of synthesis, at low cost [13, 20, 36, 37]. In the present study, for citrate gel-combustion synthesis, the following reagents were used: copper trihydrate,

$Cu(NO_3)_2 \cdot 3H_2O$ (Merck p.a.), ammonium molybdate $(NH_4)_6Mo_7O_{24} \cdot 4H_2O$ (Aldrich, p.a.) and citric acid, $C_6H_8O_7 \cdot H_2O$ (Merck p.a.). Citric acid served simultaneously as fuel and chelating agent. All chemicals were mixed in different molar ratios, $xCuO\text{-}(1\text{-}x)MoO_3$ where x was in the range from 0.1 to 0.9. The molar ratio of nitrate against citrate ions was kept approximately to be ¼, as recommended elsewhere [36, 37]. Solutions were subjected to water evaporation in an open glass beaker on a hot plate of magnetic stirrer under permanent stirring, until homogeneous dry gel was formed. The heating was then continued in an oven (LAC, LO3-15711, Czech Republic) up to the temperature of self-ignition. The temperature of self-ignition scattered somewhat about 450 °C. The ignition reaction proceeded in a form of frontal flame propagation through the dry gel. The main source of oxygen needed to citric acid combustion is the decomposition of nitrate anions. To remove carbon residues from obtained oxide mixtures, the samples were subjected to an additional heating at a constant temperature of 450 °C in air for half hour.

**Thermal analysis:** The reduction of $CuO–MoO_3$ samples were estimated by thermogravimetry (TG) using the TA SDT 2060 device for simultaneous thermogravimetry and differential thermal analysis (DTA). The working atmosphere was the gaseous mixture 25 vol.% $H_2$ in Ar provided from high-pressure tanks. The flowing rate was 80 $cm^3$ $min^{-1}$. The purity of gases used to make this gaseous mixture was 99.995 vol. %. Although the kinetic of reduction is expectedly faster in pure hydrogen, which is important for practical purposes, in the present study hydrogen diluted by argon was used for safety of the thermogravimetric device, but also to keep comparability with our former studies of $CuO\text{-}WO_3$ [13] $NiO\text{-}MoO_3$ [36], and pure CuO [20] reduction, all being considered in the Results and Discussion section.

. Usually, 10 mg of sample was poured into alumina sample pans of 90 μL volume. The samples were reduced at a single heating rate of 10 °C $min^{-1}$. Exceptionally, for the purposes of kinetic analysis, the reduction of the system $0.5CuO\text{-}0.5MoO_3$ was carried out at multiple heating rates in the range 5 - 25 °C $min^{-1}$.

**SEM characterization:** The particle size and morphology of composite oxide powders and their metallic composites obtained upon oxide reduction, were performed by both X-ray diffractometry and scanning electron microscopy. For electron microscopy SEM JEOL JSM-6390 LV was used, while X-ray diffractometry was performed by means of Phillips PW-1710 diffractometer with X-ray tube Cu 1FF working at 40 kV and 30 mA. The monochrome $Cu_{\alpha 1,2}$ line of 0.15418 nm was used for measurements. The step width angle was $0.020^o$ with the duration 0.6 s. Divergence and receiving slit apertures amounted to 1 and 0.1 mm, respectively.

## 3. RESULTS AND DISCUSSIONS

### 3.1 The characterisation of $xCuO\ (1\text{-}x)MoO_3$ samples

Before the examination of oxide mixtures reduction, we briefly checked the phase composition of the synthesized products by X-ray diffractometry. Based on the phase diagram [1], one may expect the mixture $MoO_3$ + $CuMoO_4$ in $MoO_3$-rich region of compositions, and the mixture CuO + $Cu_3Mo_2O_9$ in CuO-rich region of compositions, while pure phases $CuMoO_4$ and $Cu_3Mo_2O_9$. may be expected for x = 0.5 and 0.6, respectively. The diffractograms of selected oxide compositions were shown in Fig. 1. The diffraction lines of various phases were identified relying on the Pearsons Crystal Data (PCD) software. The most intense diffraction lines of characteristic phases found in the observed systems assigned by their Miller indices are as follows (from lowest toward higher 2θ values): for CuO (labeled by o) (PCD card No 1142013): 002, 111, 20-2, 020, 202, 11-3, 310, and 113), for $Cu_3Mo_2O_9$ (labeled by + ) (PCD card 1100053): 020, 110, 130, 031, 200, 210, 040, 131, 002, 201, 140, 022, 112, 230, 150, 240, 202, 042, 241, 142, 160, 232, 340, 071, 322, 411, 271, 040 and 432; for α-$CuMoO_4$ (black rectangles)(PCD card No 1703589): 001, 011, 002, 101, 02-1, 1-20, 012, 111, 02-2, 20-1, 2-1-2, 1-2-2, 210, 21-3, 023, 04-2, 1-42, 132, 02-5, 1-3-4, 4-1-2; for $MoO_3$ (labeled by x) (PCD card No 1252481): 001, 10-1, 002, 011, 110, 003, 20-1, 013, 020, 12-1 and 014.

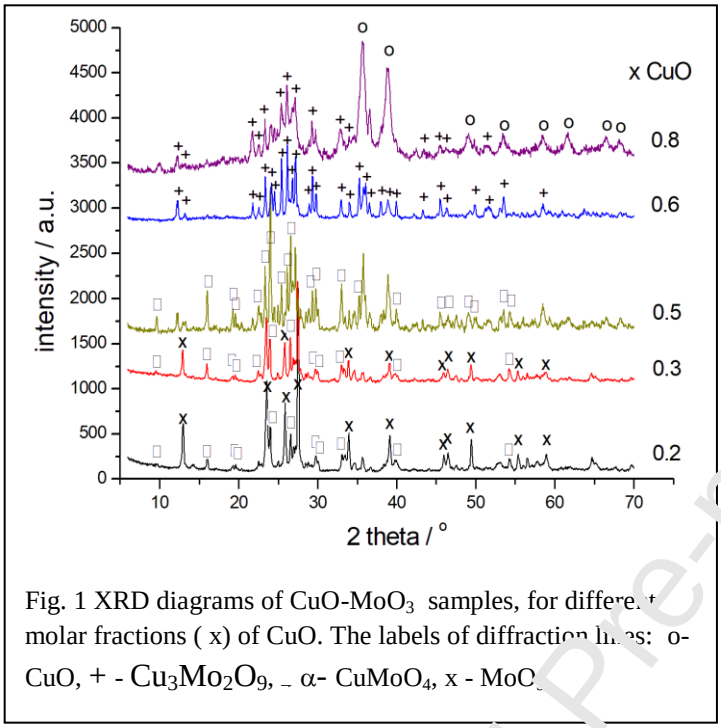


Fig. 1 XRD diagrams of CuO-$MoO_3$ samples, for different molar fractions ( x) of CuO. The labels of diffraction lines: o-CuO, + - $Cu_3Mo_2O_9$, _ α- $CuMoO_4$, x - $MoO_3$

As obvious from Fig.1, in the $MoO_3$-rich region of compositions (x equal to 0.2 and 0.3), the diffraction lines of $MoO_3$ and α-$CuMoO_4$ are present. The relative intensity of $MoO_3$ lines

decreases with the increase in CuO mole ratio from 0.2 to 0.3. For x = 0.5, α- $CuMoO_4$ phase prevails, however the remaining lines of $MoO_3$ and CuO indicate that a part of oxide reactants remained unreacted. Probably, as Benchikhi et al. [14] done, the mixture $0.5CuO\text{-}0.5MoO_3$ obtained by sol-gel procedure should be treated additionally at 500 $^oC$ in order to transform it completely into a pure α-$CuMoO_4$ phase. However, in order to keep the uniformity of synthesis procedure used in this study, that procedure was not followed. For the composition $CuO:MoO_3$ = 3:2, (x = 0.6) pure $Cu_3Mo_2O_9$ phase was identified, as expected for this molar ratio. This may mean that $Cu_3Mo_2O_9$ undergoes less kinetic hindrance of formation in comparison to α-$CuMoO_4$. A further addition of CuO produces the phase mixture $Cu_3Mo_2O_9$ + CuO, as shown in Fig. 1 for CuO mole fraction of 0.8. The appearance of α-$CuMoO_4$ and $Cu_3Mo_2O_9$ phases confirms that the gel-combustion procedure provides easy reaction between precursor components, thanks to an almost molecular homogeneity achieved [13].

The SEM images of $xCuO\text{-}(1\text{-}x)MoO_3$ samples are presented in Fig 2. The samples rich in copper oxide have the form of huge thread-like agglomerates of tiny particles being ~300 nm in diameter, like to pure CuO sample synthesized by the same gel-combustion procedure [13,

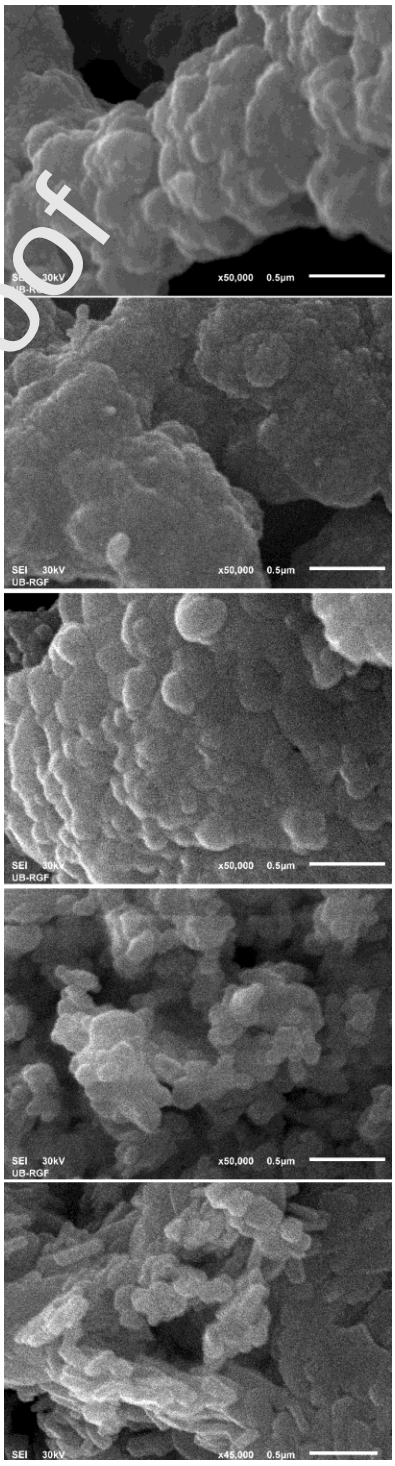


Fig 2. The SEM pictures of $xCuO\text{-}(1\text{-}x)MoO_3$ system. x (from top downwards) = 0.9; 0.7; 0.5; 0.3 and 0.1. The length of white bar is 0.1μm

20]. The compositions rich in $MoO_3$, display well grained, separated particles, characteristic of pure $MoO_3$ phase. With the enrichment in $MoO_3$, the agglomerates become smaller, and the mean particle diameter of oxide mixtures abates to approx. 150 nm.

Although one deals here with phase mixtures, CuO + $Cu_3Mo_2O_9$ in CuO-rich composition region and $MoO_3$ + $CuMoO_4$ in $MoO_3$-rich composition region, the uniform morphology obtained by gel-combustion technique does not depict this complex phase composition.

### 3.2. Thermogravimetric study of the reduction of xCuO - (1-x)$MoO_3$ oxide system

Figure 3. presents the thermogravimetric curves obtained during reduction of xCuO-(1-x)$MoO_3$

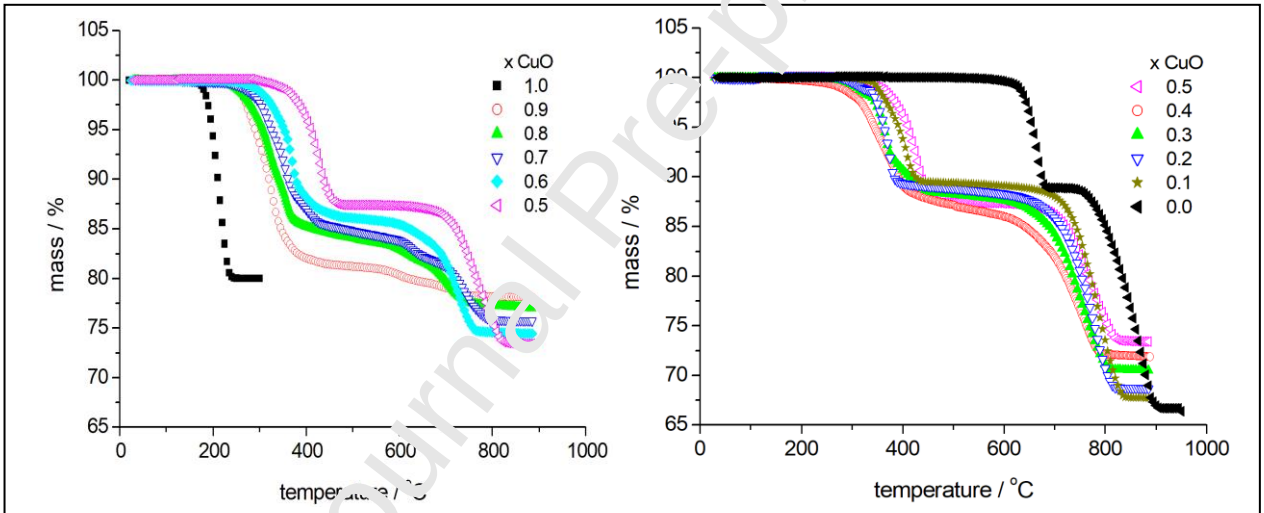


Figure 3. The TG curves of reduction of xCuO:(1-x)$MoO_3$ samples in Ar + 25% $H_2$ flow, recorded at a common heating rate of 10 °C $min^{-1}$. Left: CuO-rich region, right: $MoO_3$-rich region of compositions

samples in hydrogen atmosphere stream, for x varying between 0.1 and 0.9. To avoid overlapping of many curves and provide better visual inspection, they were divided into two diagrams, the first one covering the CuO-rich region of molar ratios and the second one covering the $MoO_3$-rich region of molar ratios. For the sake of comparison, the TG curves for pure CuO and pure $MoO_3$ were also added to these diagrams. The curve for x = 1 (pure CuO) originates from our former investigations of gel-combustion synthesis and reduction of CuO samples [13,

20]. The $MoO_3$ sample used in this study was obtained by simple thermal decomposion of $(NH_4)_6Mo_7O_{24} \cdot 4H_2O$, and subjected to reduction under the same conditions as the other samples. The TG curve of reduction of pure CuO, looks like a single step process, which upon a mass loss of 20.0 % yields metallic Cu (actual mass loss for this process calculated on the basis of stoichiometry is 20.1 %). The reduction of pure $MoO_3$ proceeds in a well known two-step process [29, 36], first one being $MoO_3 \rightarrow MoO_2$, with theoretically expected mass loss of 11.1 % (i.e., remaining mass of 88.9 %), and the second one being $MoO_2 \rightarrow Mo$, with the expected mass loss of 33.3 % (i.e., remaining mass of 66.7 %). The values obtained experimentally for $MoO_3$ reduction practically overlap with the theoretically expected ones, as shown in Fig. 3 for the case x = 0. As Fig. 3 shows, the TG curves for $0.1 < x < 0.9$ are non-uniformly distributed along the temperature axis, between the ones related to pure ingredients. One may see that the whole reduction process may be divided into the low-temperature one, taking place between 250 and 450 $^oC$, and the high-temperature one, taking place between 550 and 830 $^oC$. A plateau of low reactivity separates these regions.

Fig 3 shows that the mass loss in the low-temperature region is equal or higher from the mass of metallic Cu which may be obtained by reduction of total CuO present in the system. Thus we anticipated that in this region the following two reactions (I and II) may take place:

$$CuO + H_2 = Cu + H_2O \qquad (I)$$

involving both free CuO and that bonded with $MoO_3$ within either $Cu_3Mo_2O_9$ or $CuMoO_4$ phase, and

$$MoO_3 + H_2 = MoO_2 + H_2O \qquad (II)$$

involving either free $MoO_3$ or that liberated upon CuO reduction from $Cu_3Mo_2O_9$ or $CuMoO_4$ phases.

In the high-temperature region, we anticipated the preferable reaction is:

$$MoO_2 + 2H_2 = Mo + 2H_2O \qquad (III)$$

The Table I was constructed in order to prove these assumptions. Calculated mass losses for reactions (I) and (II) separately, are presented in the second and the third column while the sum of mass losses is shown in the fourth column of Table I. The calculated sum is compared to the experimentally determined one (fifth column), read as the positions of the plateaus separating the

Table I. The mass loss, (%) for reduction of CuO , and low-temperature reduction step of $MoO_3$ (lts), their sum calculated and determined experimentally and actual mass upon complete reduction, calculated ($m_{tot}$, %) and experimentally determined ($m_{tot}$, % exp.)

| xCuO | $\Delta m_{CuO}$, % calc. | $\Delta m_{MoO3}$(lts),% calc. | $\Delta m_{CuO}+\Delta m_{MoO3}$(lts), % calc. | $\Delta m_{CuO}+\Delta m_{MoO3}$(lts), % exp. | $m_{tot}$, % calc | $m_{tot}$, % exp. |
|---|---|---|---|---|---|---|
| 1.0 | 20.1 | 0.00 | 20.1 | 20.0 | 79.90 | 80.0 |
| 0.9 | 18.1 | 1.11 | 19.2 | 18.5 | 78.57 | 78.2 |
| 0.8 | 16.09 | 2.22 | 18.3 | 16.1 | 77.24 | 77.1 |
| 0.7 | 14.08 | 3.33 | 17.4 | 15.0 | 75.92 | 76.8 |
| 0.6 | 12.07 | 4.44 | 16.5 | 14.0 | 74.59 | 74.5 |
| 0.5 | 10.06 | 5.55 | 15.6 | 12.5 | 73.27 | 73.4 |
| 0.4 | 8.045 | 6.66 | 14.7 | 13.0 | 71.96 | 71.9 |
| 0.3 | 6.03 | 7.77 | 13.8 | 12.0 | 70.67 | 70.6 |
| 0.2 | 4.02 | 8.88 | 12.9 | 11.5 | 69.31 | 68.7 |
| 0.1 | 2.01 | 9.99 | 12.0 | 10.8 | 67.99 | 67.8 |
| 0.0 | 0.00 | 11.1 | 11.1 | 11.2 | 66.7 | 66.6 |

temperature regions in Fig 3. Also the remaining sums of masses after completing all three reactions (I) - (III) were both calculated (sixth column), and determined experimentally as the height of the finishing plateaus in Fig 3 (seventh column). A fair agreement between the last two columns in Table I witnesses the reliability of the thermogravimetric measurements performed in this study. However the discrepancies between the mass differences sums in fourth and fifth columns of the Table I, rising on approaching the middle region of mole ratios, indicate that the

reactions II does not complete in the low-temperature region. Therefore, in the next sections, the mechanism anticipated by the reactions (I) - (III) was refined, taking into consideration also the derivatives of TG curves, presented in Fig 4.

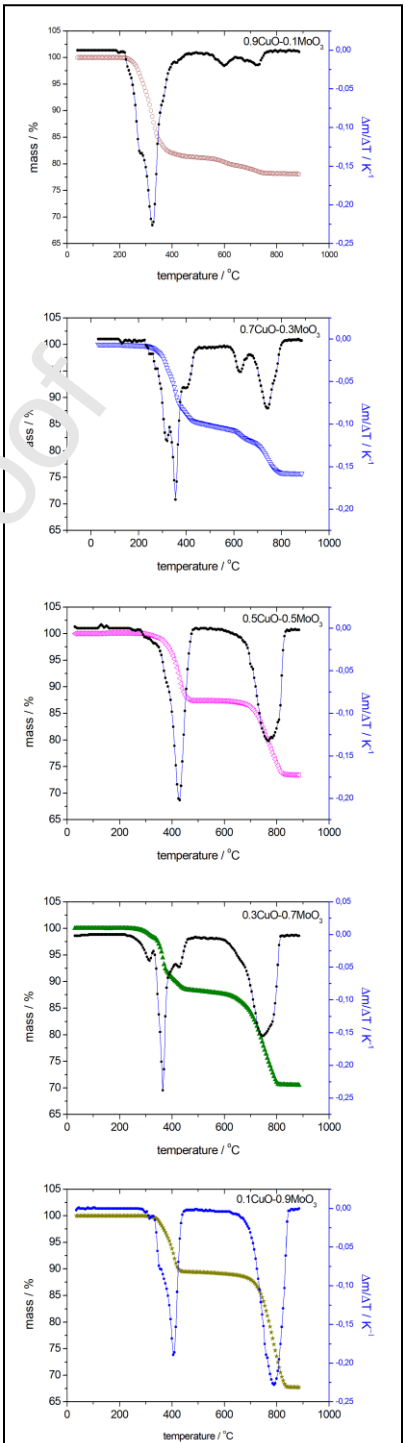


Fig 4. The TG diagrams of selected $xCuO-(1-x)MoO_3$ compositions, with their first order derivatives

3.2.1. CuO-rich composition region

In the CuO-rich region of compositions, the system CuO-$MoO_3$ may be described as the $Cu_3Mo_2O_9$ phase dispersed within an excess of free CuO. According to the second and third columns of Table 1, for large CuO mole ratios (x = 0,9 - 0.7) the mass loss in the low-temperature region of reduction, determined experimentally, corresponds well to the reduction of complete CuO present in the system to metallic state. This means the reduction of free CuO is accompanied by simultaneous extraction of copper from $Cu_3Mo_2O_9$, i.e. liberation of $MoO_3$.

$$Cu_3Mo_2O_9, + H_2 = Cu + MoO_3 + H_2O \qquad (IV)$$

The main peak of DTG curve representing low-temperature reduction region possess two bulges (Fig 4, top two diagrams) visible particularly for x = 0.7. The first one may mean the appearance of intermediate $Cu_2O$ phase, which is

already known from the literature [17]. The second one may be attributed to the beginning of extraction of Cu by decomposition of $Cu_3Mo_2O_9$

It seems that complete $MoO_3$ liberated by reaction (IV) undergoes reduction within the high-temperature reduction region. This is recognizable by two high temperature peaks in Fig 4, characteristic of two-step reduction of pure $MoO_3$, visible in upper two derivative TG diagrams in Fig 4. Both reduction steps start at considerably lower temperatures than in the case of pure $MoO_3$, which may be a manifestation of the catalytic action of metallic coper.

3.2.2. Equimolar oxide system, $0.5CuO\text{-}0.5MoO_3$

As x approaches 0.5, rising part of $MoO_3$ liberated by complex oxide reduction/decomposition (reaction IV), undergoes first step reduction (i.e. reaction II) in the low-temperature region together with CuO. For instance (see fourth column in Table I), for x = 0.5, where complex oxide composition is mainly $CuMoO_4$, theoretically expected mass loss for CuO + ($MoO_3 \rightarrow MoO_2$) reduction is 10.06 + 5.55 = 15.6, i.e., remained total mass of non-volatile products of the reactions (I) and (II) amounts to 84.4 %. The height of corresponding middle plateau in Fig 3 is 87.5 %. This means that 3.1 % (of expected 5.55 %) of mass loss during the $MoO_3 \rightarrow MoO_2$ reduction step is realized in the low-temperature region, while remaining 2.45% of mass loss is realized in the high-temperature region. The remaining fraction of the $MoO_3 \rightarrow MoO_2$ reduction step continues to the $MoO_2 \rightarrow Mo$ one. Both these steps produce an apparently unique high-temperature peak of DTG curve (middle diagram in Fig 4) however, its complexity manifests itself by its broadness and asymmetry.

3.2.3 $MoO_3$ –rich composition region

The $MoO_3$-rich composite region of CuO-$MoO_3$ system may be interpreted as the mixture of $CuMoO_4$ finely dispersed within the excess of $MoO_3$. With lowering of CuO mole fraction below x = 0.5, the relatively large mass loss in the low-temperature reaction region is explainable only by rising part of the $MoO_3 \rightarrow MoO_2$ reduction along with the formation of metallic copper. For instance, for x = 0.1 the initial formation of Cu particles is followed by $MoO_3 \rightarrow MoO_2$ reduction. The bulge on the low-temperature endothermic peak denotes the finishing of Cu liberation from $CuMoO_4$ i.e. the disappearance of this phase. In this case, as presented in fifth column of Table I, the actual total mass loss in the low-temperature reaction region is 10.8 %, which is only for 1.2 % lower from the total mass drop calculated for reactions (I) and (II). This means further that $MoO_2 \rightarrow Mo$ presents the dominating part of the high-temperature reduction process, which sounds with the symmetrical shape of the derivative of TG curve in the high-temperature region (bottom diagram in Fig. 4).

3.2.4. Catalysis/inhibition interactions in the reduction of CuO-$MoO_3$ system

The inspection of the TG curves in Fig 3 in CuO-rich composition region indicates a strong inhibition of CuO reduction caused by the presence of $MoO_3$ in the system. For xCuO = 0.9 the mean reduction temperature is shifted for 100 $^oC$ toward higher temperatures in comparison to the reduction temperature of pure CuO. The shift of the onset of CuO reduction may not be attributed to the formation of $Cu_3Mo_2O_9$, since complete CuO experiences reduction inhibition. It seems that the influence of Mo-O bond making $MoO_3$ difficult reducible in comparison to Cu-O bond, is not limited to $Cu_3Mo_2O_9$ phase only, but spreads over the whole oxide system emphasizing also large existing excess of free CuO. This may be the consequence of volatility of $MoO_3$, the vapors of which may cover whole oxide mixture during gel-combustion procedure or during additional thermal treatment of synthesis procedure. Namely $MoO_3$ displays measurable

vapor pressure already at 500 C [38], and its volatilization is particularly enhanced in presence of moisture (developed always during the gel-combustion procedure), due to the formation of $MoO_2(OH)_2$ [39]. With increasing mole fraction of $MoO_3$ up to 0.5, the mean reduction temperature shifts commensurably toward higher values.

On the other hand, metallic Cu, appearing in the low-temperature reduction region, displays strong catalytic effect on the reduction of $MoO_3$. In the CuO-rich composition region this effect is visible as the shift of both reduction steps of $MoO_3$ toward lower temperatures in comparison to pure $MoO_3$ (see upper two diagrams in Fig 4). At $x$ values equal or larger than 0.5, one may observe huge catalytic effect of copper on the first step reduction of $MoO_3$, causing the shift of mean reduction temperature for 280 $^oC$ toward lower temperatures, in comparison to the first reduction step of pure $MoO_3$. On the basis of these results, one may expect also considerable acceleration of $MoO_3$ reduction if mixed, for instance by ball milling, with fine Cu powder.

Probable explanation of catalytic effect of Cu is dissociation of hydrogen adsorbed on Cu surface (which is site and plane orientation sensitive), and its spillover on $MoO_3$ or $MoO_3$-containing compounds [40-42]. This assumption is supported by the fact that the effect is mostly pronounced at small mole fraction of Cu. Namely, at small fractions of Cu, the Cu particles obtained by reduction are dispersed on a relatively large solid $MoO_3$ surface, which prevents its agglomeration, and keeps it in the stage of high specific surface area. On contrary, in CuO-rich composite region, a pronounced temperature assisted agglomeration of Cu into coarse droplets mitigates its catalytic activity.

3.2.5. Comparison with the reduction process of similar oxide systems

The here observed system shows particularities of reduction mechanism in comparison to the system CuO-$WO_3$. studied previously in the same way [13]. Namely, in the CuO-$WO_3$ system, the reduction of CuO to Cu, is always clearly separated from the two reduction steps of $WoO_3$, namely, $WO_3 \rightarrow WO_2$, and $WO_2 \rightarrow W$ ones. This difference may be explained by means of thermodynamic properties of considered oxides. Namely, according to tables of thermodynamic properties [43], free energies of formation ($\Delta G_f$) of CuO, $MoO_3$, $WO_3$ and $H_2O$ are -129.7, -666, -764, and -237.1 kJ $mole^{-1}$, respectively, or, per one oxygen atom. -129.7, -222.7, -255.6 and -237 kJ $mole^{-1}$, respectively. The differences

$\Delta G_f(H_2O) - \Delta G_f(CuO) = -237.1 - (-129,7) = -107.4$ kJ $mol^{-1}$

and

$\Delta G_f(H_2O) - \Delta G_f(MoO_3$, per O atom$) = -237.1 - (-227.7) = -9.4$ kJ $mol^{-1}$

are negative numbers, i.e. these reactions are spontaneous under standard conditions. On the other hand, the difference:

$\Delta G_f(H_2O) - \Delta G_f(WO_3$, per O atom$) = -237.1 - (-255,6) = 18.5$ kJ $mol^{-1}$

is positive, thus within a mixture CuO-$WO_3$ under standard conditions only CuO reduction is thermodynamically allowed. Thus, upon separation of Cu as a pure phase, $WO_3$ reduction steps may take place only thanks to the removal of $H_2O$ by $H_2$+Ar stream, which shifts the mean temperature of the reaction:

$$WO_3 + 3H_2 = W + 3H_2O \qquad (V)$$

towards the low-temperature direction.

Different behavior during reduction shows also the NiO-$MoO_3$ system [36]. Although NiO, similarly to CuO, is easily reducible by hydrogen (reduction takes place between 280 and 400 $^oC$, at heating rate 10 $^oC$ $min^{-1}$), the TG curves show that the mean reduction temperature

increases more monotonously along temperature axis as molar fraction of $MoO_3$ increases, i.e. there was no any discontinuity between the low- and the high-temperature reduction regions. Brito et al. [46], studying the alumina-supported NiO-$MoO_3$ catalyst, claimed that the adsorption of $H_2$ and its dissociation on Ni surface stimulated reduction of $MoO_3$. In NiO-$MoO_3$ system [36] even small molar fraction of NiO almost erases the temperature difference between $MoO_3 \rightarrow MoO_2$ and $MoO_2 \rightarrow$ Mo reduction steps. Difference between CuO-$MoO_3$ and NiO-$MoO_3$ system may originate from the difference between solubilities of reduction products. While Cu is insoluble in Mo, Ni and Mo build a series of solid solutions and intermetallic compounds, thus the appearance of metallic Ni accelerates the appearance of Mo through the free energy of intermetallic interactions.

The thermodynamic data about the stable phases inside the very system CuO-$MoO_3$ are either scarce ($CuMoO_4$) [44, 45], or non-existing ($Cu_3Mo_2O_9$). Levchenko et al. [44] by high-temperature calorimetry determined the heat of formation of $CuMoO_4$ from CuO and $MoO_3$ under standard conditions to amount to -49.7 (± 3) kJ $mol^{-1}$. Thus the enthalpy of formation of $CuMoO_4$ from the elements may be determined as the following sum:

$\Delta H°_f (CuMoO_4) = \Delta H°_f (CuO) + \Delta H°_f (MoO_3) + (-49.4) = -\ 943.4.$ kJ $mol^{-1}$

Recently, using density functional theory (DFT) method, Yu-jing et al. [45] calculated the enthalpy of formation of $CuMoO_4$ to amount to -1058.45 kJ $mol^{-1}$. The DFT value is appreciably different than the value obtained from experimental data, thus the last one should be treated as more reliable.

The gain in thermodynamic stability of $CuMoO_4$ with respect to the sum of formation enthalpies of CuO and $MoO_3$ in amount of -49.6 kJ $mol^{-1}$ may be a reason for the deceleration of its reduction, i.e., for the right-hand shift of reduction temperature, in comparison to that of pure

CuO. Although not examined, one may expect similar stabilization effect to be the reason of deceleration of $Cu_3Mo_2O_9$ reduction versus the CuO one, too.

### 3.3 Kinetics of reduction of 0.5CuO - 0.5$MoO_3$ sample

The reduction of a particular sample, synthesized of equimolar mixture of CuO and $MoO_3$, for which the reduction processes in low- and high-temperature reaction regions are visually well separated is selected to be analysed from the kinetic point of view. This sample is preferably in the stage of α-$CuMoO_4$, and its low-temperature reduction step (finishing up to 450 °C ) can be generally described as an extraction of Cu under liberation of $MoO_2$ + $MoO_3$ mixture, by the chemical equation:

$$CuMoO_4 + (1+y)H_2 = Cu + (yMoO_2 + (1-y)MoO_3) + (1+y)\,H_2O \qquad (VI)$$

where y is molar fraction of $MoO_3$ reduced to $MoO_2$ in the low-temperature region. According to the TG derivative in Fig 4, this reaction hints an one-step process. The high-temperature reduction step (observed in the region 550-960 °C) corresponds to a reduction of non-reduced part of $MoO_3$ to $MoO_2$ which continues to the reduction of $MoO_2$ to metallic Mo. In Fig 4, (derivative of TG curve for x = 0.5), complete high-temperature processes look like also to be an unique reduction step.

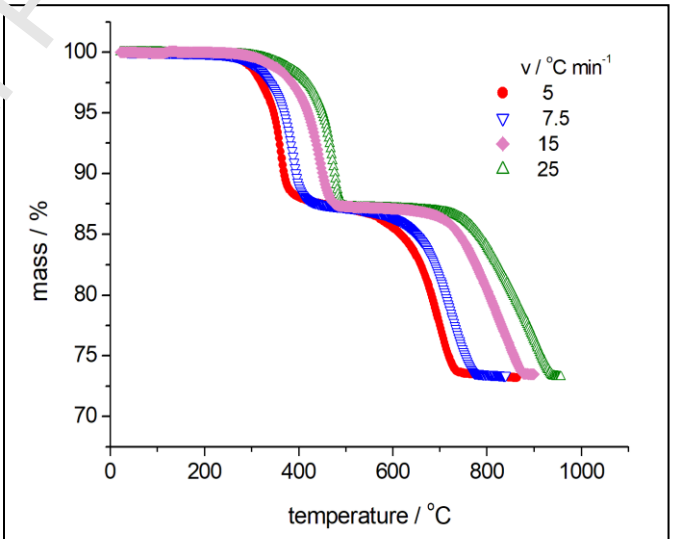


Fig 5. The TG curves of reduction of 0.5CuO-0.5$MoO_3$ at various heating rates

Fig 5 shows the TG curve of reduction of this sample at four heating rates 5, 7.5, 15 and 25 °C $min^{-1}$. As regularly, the TG curves shift toward higher temperatures as the heating rate increases.

For kinetic analysis the relative mass change is transformed into dimensionless conversion degree, alternatively called fraction reacted, α, by means of equation:

$$\alpha = \frac{m_0 - m_t}{m_0 - m_f} \quad (1)$$

where $m_o$ is initial mass fraction (100 %), $m_t$ actual mass fraction and $m_f$ final mass fraction, usually recognized as finishing plateau of TG curve.

The kinetic parameters. i.e. preexponential factor and energy of activation, which specify the standard Arrhenius equation of reaction rate, were calculated on the basis of expanded Friedman isoconversional method expressed by the equation [47]:

$$\ln\left(\frac{d\alpha}{dt_\alpha}\right) = -\frac{E_\alpha}{RT_\alpha} + \ln\{A_\alpha f(\alpha)\} \quad (2)$$

Here $t_\alpha$, $T_\alpha$, $E_\alpha$ and $A_\alpha$ are time, temperature, apparent activation energy and pre-exponential factor, respectively at a given conversion degree α.

In this study, for the kinetic analysis software Kinetics2015 was used [48].

The method based on Eq 2 uses the mass vs. T dependence determined at several heating rates. The plot $\ln(d\alpha/dt_\alpha)$ vs. $1/T_\alpha$ for fixed α enables to determine the slope $-E_\alpha/R$, while the intercept at the vertical axis, amounts to $\ln[A_\alpha f(\alpha)]$. The intercept may be used to calculate preexponential factor A, however for that purpose the mathematical form for the reaction model $f(\alpha)$ should be assumed. The method based on Eq. 2 assumes $f(\alpha)$ is equal to first power of α.

If in the observed system the assumption that f(α) is equal to α is actually fulfilled, the pairs A and $E_\alpha$ would be invariant of α.

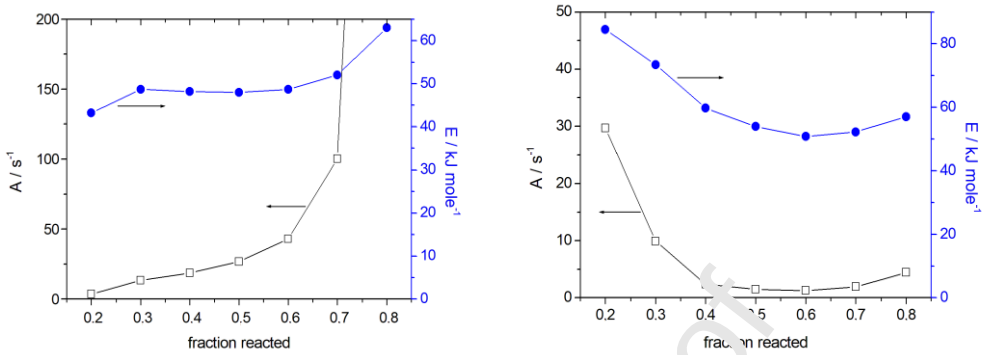


Figure 6. The dependence of preexponential factor A (empty squares) and energy of activation E (full circles) on the fraction reacted, obtained by expanded Friedman isoconversional method, for low-temperature (left) and high-temperature (right) region of reduction of 0.5 CuO - 0.5 $MoO_3$ oxide system

Since the reduction of the observed system proceeds in two well separated temperature regions, in order to simplify analysis, these regions were analysed separately.

Figure 6. shows the dependence of $E_\alpha$ (solid line) and A (dotted line) with conversion degree α for both reduction regions visible in Fig.1, in conversion degree region 0.2 - 0.8, which is considered as reliable in thermogravimetric measurement of reaction kinetics. Evidently, both A and $E_\alpha$ fluctuate significantly with the variation in α. Often these values are linearly correlated, through the so called compensation effect, lnA = a + bE, where a and b present compensation constants [49]. By means of the discrete model, an option in the Kinetics2015 software, the following correlations were obtained, for low-temperature reduction region:

$$\ln A = -0.192 + 4.04 \cdot 10^{-4} E_\alpha$$

and for high-temperature reduction region:

$$\ln A = 0.424 + 1.54 \cdot 10^{-4} E_\alpha$$

Multi-heating rate procedures, as is that used in this study, are intended to independent determination of these kinetic parameters in the presence of compensation effect. With these pairs of A and $E_\alpha$ values for given $\alpha$ values one can turn back attempting to calculate TG curves and compare them with experimental ones. Fig 7 shows the comparison of calculated (solid lines) and experimental (symbols) curves in a form of dependence of fraction reacted, $\alpha$, on temperature, for both low and high-temperature regions. The error data of the fitting procedure, i.e., the sum of squares of weighted normalized cumulative residuals (RSS) are 0.284 and 0.326 for low- and high-temperature reaction regions, respectively. This is relatively good fit, and main contribution to the RSS magnitude stems from the discrepancy appearing at heating rate 15 $^{o}$C min$^{-1}$.

Generally, if A and $E_\alpha$ obtained by isoconversional method vary with the variation in fraction reacted $\alpha$, it is indication that $f(\alpha)$ differs from $\alpha$, (i.e. from a first power reaction model) and then some other reaction model from group of the model-fitting ones [50] should be solicited. In oxide reduction reactions extended Prout-Tompkins model introduced by Burnham

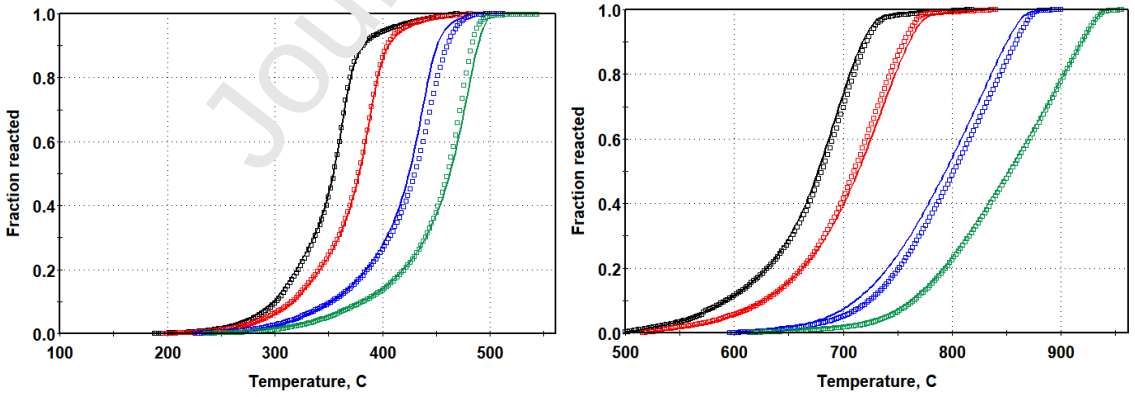


Figure 7. Experimental (symbols) and simulated (solid lines) dependence of conversion degree on temperature for low-temperature (left) and high-temperature (right) reaction regions of 0.5 CuO-0.5 $MoO_3$ oxide mixture: the heating rates (from left toward right) 5, 7.5 , 15 and 25 °C min$^{-1}$

et al. [51] to simulate nucleation-growth processes, was successfully applied [13, 20]. A

nucleation-growth model assumes that the generation of small aggregates or clusters of the new phase is the rate-determining step. Nucleation and growth models in practical situations may be unified by extended Prout-Tompkin's model, introduced by Burnham and Braun [52]:

$$\frac{d\alpha}{dt} = k\left(1-\alpha\right)^{n}\left(1-q(1-\alpha)\right)^{m}, \tag{3}$$

where $q$ is a an initiation parameter, while $m$ represents parameter related to the growth dimensionality or brancing ratio, depending on whether the reaction is a solid-state or fluid-solid reaction. Burnhan and Braun [52] set $q$ value at 0.99, but it is an arbitrary term.

This model anticipates sigmoidal dependence of isothermal alpha versus time dependence, likely as for autocatalytic reactions. For instance, Sloczynski et al. [28]. described the reduction of $MoO_3$ as an autocatalytic reaction.

Alternatively, phase boundary controlled reaction models were suitable for oxide reduction processes. In phase boundary controlled models, a rapid nucleation leading to the formation of an uniform layer of the reduction product around the oxide particle, and its contraction at a constant rate is assumed [53]. However, for the low-temperature region, none of here mentioned reaction models did not enable better fit from that achieved by isoconversional method. In other words, any other model gave higher and much higher RSS values. Thus, we have calculated activation energy by means of two additional isoconversional models: expanded Kissinger and Flyn-Wall-Ozawa (FWO), in order to confirm that the isoconversional analysis is the most suitable in this case. The Flynn–Wall–Ozawa isoconversional (FWO) method is based on the equation [54,55]:

$$\ln(\beta) = \ln\left[A\frac{f(\alpha)}{(d\alpha/dT)}\right] - \frac{Ea}{RT} \tag{4}$$

For a constant conversion, a plot of ln β versus 1/T, from the data at different heating rates, leads to a straight line whose slope provides Ea calculation.

The Kissinger method [51, 56, 57] is a special isoconversional case of determining A and $E_\alpha$ at a fixed conversion degree, based on the equation:

$$\ln\frac{\beta}{T_{max}^2} = \ln\frac{AR}{Ea} - \frac{Ea}{RT_{max}} \quad (5)$$

where $T_{max}$ is temperature of maximum reaction rate. The plot $\ln(\beta/T_{max}^2)$ vs. $1/T_{max}$ at different heating rates, β, gives a straight line having the slope equal to $-E_\alpha/R$, and the intercept involves the value of preexponential factor A.

By expanded Kissinger method, $E_\alpha$ was found to amount to ~ 44 kJ mol$^{-1}$ , while FWO gave 55 kJ mol$^{-1}$ . Both results are in compliance with the $E_\alpha$ value obtained by expanded Friedman method (47 kJ mol$^{-1}$) for low temperature reaction region. For the high-temperature region, in which $MoO_3$ reduction reaction dominates, model-fitting nucleation and growth model gave good fit and satisfactory results, with the following kinetic parameters: $E_\alpha$ = 65 kJ mol$^{-1}$, A = 5.54 s$^{-1}$, m = 0.47 and n = 0.52, and with RSS 0.6423. This $E_\alpha$ value corresponds well to that obtained by Friedman method (65.4 kJ mol$^{-1}$). For the sake of comparison, we present also the values obtained by expanded Kissinger (59.9 kJ mol$^{-1}$) and FWO (81.3 kJ mol$^{-1}$) methods. Nucleation and growth model for reduction process of neat $MoO_3$ was confirmed previously in the literature [36], but much higher $E_\alpha$ values published there witnesses that copper is an effective catalyst in $MoO_3$ reduction process. Similar conclusion on copper action was derived for NiO-$MoO_3$ system if reduction agent was carbon monoxide [58].

It is noteworthy that the values of activation energies, being approx. 50 – 80 kJ mol$^{-1}$ (Fig. 6), are not strange for transition metal oxide reduction, however, the values of preexponential factor, being 1-1000 in magnitude order, are too small for any real physical picture of oxide reduction

reaction, and indicate a complex nature of the related reduction process, in spite of visual simplicity following from TG curve derivative visible in Fig.4.

### 3.4 **The XRD and SEM characterization of reduction products**

Although the correspondence of mass loss predicted theoretically for total elimination of oxygen according to the equations (I-III), to that determined experimentally (see last two columns in Table 1), may be considered as a reliable evidence that the reduction products are pure metallic Cu-Mo composites, we checked that assumption additionally by X-ray diffractometry. Fig. 8 shows the X-ray diffractogram of phases obtained upon the $CuO - MoO_3$ oxide mixture reduction. Main diffraction lines of pure Mo (body centered cubic cell, PCD card 1933225. lines 110, 200, 211 and 220) and pure Cu (cubic close-packed cell, PCD card 1826483, lines 111 and 200, 220 (last one being masked by 211 Mo line) phases were observed, which evidence that metallic composite system Cu – Mo is obtained. The lines of Cu show uniform intensity increase with the increase of molar fraction of Cu. In the 0.7Cu-0.3Mo system some additional peaks appear indicating the traces of $Cu_2O$. This is easily

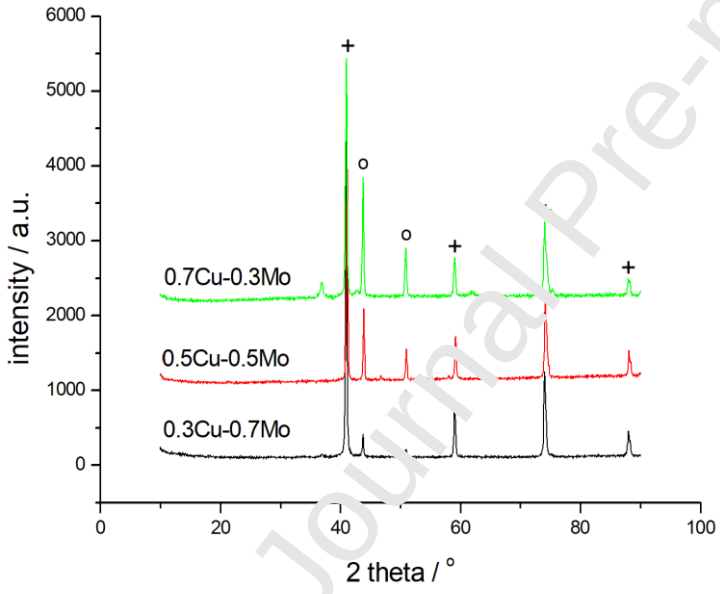


Fig 8. X-ray diffractogramms of Cu-Mo composites. The Mo lines are labeled by crosses and Cu lines by circles.

explainable, since one deals with the finely dispersed powders, which are prone to build surface oxides if stored in air even at room temperature.

Fig. 9 shows the SEM pictures of obtained metal composites of selected mole ratios. In the cases when CuO prevailed in the oxide mixture, the droplet-like Cu particles are visible. This is the consequence of the fact that the reduction of CuO happens much earlier than the reduction of $MoO_2$, and waiting to the onset of $MoO_2$ reduction, majority of metallic copper accumulates into droplets through solid state diffusion gathering and sintering. The radii of droplets, amounting up to several microns for x = 0.9, and up to 2 microns for x = 0.7, abate with further decrease in CuO mole fraction. At small mole fractions of CuO, thanks to a large Cu vs $MoO_2$ and Cu vs. Mo surface area ratios in low- and high-temperature reaction region, respectively, the agglomeration is effectively suppressed. Therefore the composites show higher homogeneity, and the mean particle size is determined preferably by the size of thin Mo particles. High dispersion of Cu phase in this case is in sound with its high catalytic activity in $MoO_3$ and $MoO_2$ reduction.

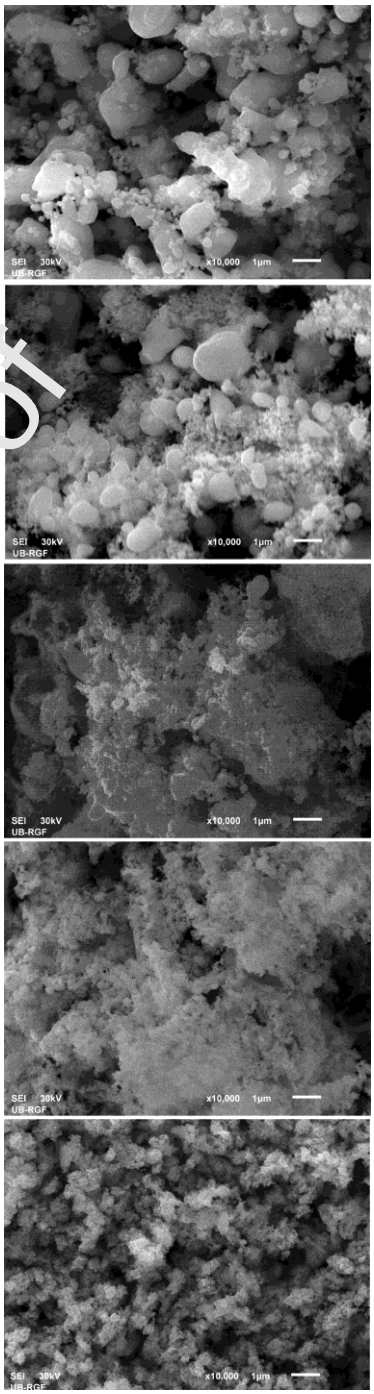

Fig 9. The SEM pictures of xCu-(1-x)Mo composites: X (from top downwards) = 0.9, 0.7, 0.5, 0.3 and 0.1. The length of white bar is 1 μm

## CONCLUSIONS

The intimate oxide mixtures xCuO-(1-x) $MoO_3$ ($0.1 \leq x \leq 0.9$) were synthesized by citrate gel-combustion method. The X-ray

diffractometry confirmed the formation of complex oxides $Cu_3Mo_2O_9$ and $CuMoO_4$ in CuO- and $MoO_3$-rich composition region, respectively The reduction of these oxide systems by gaseous hydrogen was investigated by thermogravimetry in constant heating rate regime.

The obtained TG diagrams together with their first derivatives revealed the two well separated temperature regions of reduction processes. For CuO-rich compositions, the low-temperature reduction reaction is mainly CuO reduction (involving also CuO originating from $Cu_3Mo_2O_9$ decomposition) resulting in metallic Cu, and the high-temperature reduction reactions mainly involve two-step reduction of $MoO_3$: $MoO_3 \rightarrow MoO_2$ and $MoO_2 \rightarrow Mo$ ones, resulting in metallic Mo. For $MoO_3$-rich compositions, the low-temperature reaction region involves CuO reduction originating from $CuMoO_4$ decomposition together with a part of first step of $MoO_3$ reduction, while the high-temperature reduction region involves completion of $MoO_3$ reduction to metallic Mo.

The interactions between the constituents of reaction system lead to the inhibition of CuO reduction and to the huge acceleration of $MoO_3$ reduction. The particularity in relation to the CuO-$WO_3$ system is explained in terms of differences between reducibility of $WO_3$ and $MoO_3$, while particularity in relation to NiO-$MoO_3$ system is explained by mutual solubility of nickel and molybdenum.

The reduction of equimolar oxide mixture (x = 0.5), was subjected to kinetic analysis. Among several thermoanalytical methods, the isoconversional "model-free" method enabled the best fit of all experimental data. However, model-fitting nucleation and growth model proved to be adequate for the high-temperature reduction region.

The particle size and morphology of obtained metallic xCu-(1-x)Mo composite depend on the composition. Since metallic copper separates itself much before completion of molybdenum oxide reduction, it suffers huge particle coarsening in CuO rich composition region, when micron-sized droplet-like Cu particles were observed. However, in $MoO_3$-rich samples, copper agglomeration is suppressed and it remains homogeneously distributed over fine submicron-sized Mo particles.

Acknowledgement

This study is supported by the Ministry of Education, Science and Technological Development of Republic Serbia (contract No. 451-03-68/2020-14/200146), and by Serbian Academy of Sciences and Arts (project No. F-190). D.J. is thankful to the Ministry for Scientific and Technological Development, Higher Education and Information Society of Republic of Srpska for supporting the study through the project No. 19.032/961-78/19.

**REFERENCES**

[1] T. Machej, J. Ziolkowski, Phase diagram of the CuO-$MoO_3$ system, Mater. Chem. 4 (1979) 113-122, doi:10.1016/0390-6035(79)90057-9.

[2] R.A. Prokopowicz, P.L. Silveston, R.R. Hudgins, D.E. Irish, Oxidation of carbon monoxide over a copper(II) oxide catalyst, React. Kinet. Catal. Lett. 37 (1988) 63–70, doi:10.1007/BF02061711.

[3] L. Li, D. Mao, J. Yu, X.J. Guo, Highly selective hydrogenation of $CO_2$ to methanol over CuO–ZnO–$ZrO_2$ catalysts prepared by a surfactant-assisted co-precipitation method, J. Power Sources 279 (2015) 394- 404, doi:10.1016/j.jpowsour.2014.12.142.

[4] C.-H. Wang, $Al_2O_3$-supported transition-metal oxide catalysts for catalytic incineration of toluene, Chemosphere 55 (2004) 11-17, https://doi.org/10.1016/j.chemosphere.2003.10.036.

[5] C.-H. Wang, H.-S. Weng, $Al_2O_3$-Supported Mixed-Metal Oxides for Destructive Oxidation of $(CH_3)_2S_2$, Ind. Eng. Chem. Res. 36 (1997) 2537-2542. doi:10.1021/ie960787v.

[6] E.V. Soltys, Kh. Kh. Urazov, T.S. Kharlamova, O.V. Vodyankina, Redox and catalytical Properties of Copper Molybdates with Various Composition, Kinet. Catal.+. 59 (2018) 58-69, doi:10.1134/S0023158418010111.

[7] W.M. Shaheen and M.M. Selim Characterization and Catalytic Properties of a Series of CuO-$MoO_3$ Mixed Oxides, Egypt. J. Chem. 60, (2017) 627 – 637, DOI :10.21608/ejchem.2017.1062.1052

[8] L. Zhang, W. He, Y. Liu, M. Ling, P. Zheng, S. Guo, 3D hierarchical flower of copper molybdate $Cu_3Mo_2O_9$: Synthesis, nanostructure and lithium storage properties, J. Alloys Compd. 723 (2017) 512-519, doi:10.1016/j.jallcom.2017.06.175.

[9] B. Swain, D.H. Lee, J.S. Kim, D.W. Kim, K.S. Park, Synthesis of flower - like $Cu_3[MoO_4]_2O$ from $Cu_3(MoO_4)_2(OH)_2$ and its application as an anode material for LIB: analysis of structure - electrochemical property relationships, ChemElectroChem 4 (2017) 2608‑2617, doi:10.1002/celc.201700499

[10] M.P. Pechini, Method of Preparing Lead and Alkaline Earth Titanates and Niobates and Coating Method Using the Same to Form a Capacitor, US Patent No. 3, 330, 697

[11] P. Song, J.G. Cheng, L. Wan, J.S. Yhao, Y.F. Wang, Y.B. Cai, Preparation and characterization of Mo-15 Cu superfine powders by a gelatification-reduction process, J.Alloys. Compd. 476 (2009) 226-230, https://10.1016/j.jallcom.2008.09.097.

[12] M. Zhao, J. Wang, M Zhou, Preparation and reduction behavior of MoCu powders by sol-gel, J. Phys.: Conference Series. 188(2009) 012020, https://doi.org/10.1088/1742-6596/188/1/012020.

[13] D. Jelic, S. Zeljkovic, S. Mentus, Thermogravimetric study of the reduction of CuO -$WO_3$ oxide mixtures in the entire range of molar ratios, J. Therm. Anal. Calorim. 132 (2018) 77-90, doi:10.1007/s10973-017-6921-0.

[14] M. Benchikhi, R. el Quatib, S. Guillemet-Fritsch, J.Y. Chane Ching, L. Er-Rakho, B. Durand, Sol-gel synthesis and sintering of submicronic copper molybdate($\alpha$-$CuMoO_4$) powders, Ceram. Int. 40 (2014) 5371-5377, doi:10.1016/j.ceramint.2013.10.118.

[15] S. Mitchell, A. Gomez Aviles, C. Gardner, W. Jones, Comaparative study of the synthesis of layered transition metal molybdates, J. Solid State Chem. 183 (2006) 198-207, https://doi.org/10.1016/j.jssc.2009.10.011.

[16] H. Kirakosyan, T. Minasyan, O. Niazyan, S. Aydinyan, S. Kharatyan, DTA/TG study of CuO and $MoO_3$ co-reduction by combined Mg/C reducers, J. Therm. Anal. Calorim. 123 (2016) 35–41, DOI 10.1007/s10973-015-4919-z

[17] M.S. Yazdi, M.F. Noghani, A. Najari, Mechano-chemical activation of $MoO_3$-CuO/C powder mixture to synthesis nano crystalline Mo-Cu alloy, JUFGNSM 51 (2018) 153-162, doi:10.22059/jufgnsm.2018.02.

[18] A. Sun, X. Dong, X. Wang, B. Duan, D. Wang, Synthesis of novel core–shell Cu@Mo nanoparticles with good sinterability, J. Alloys Compd. 555 (2013) 6-9, http://dx.doi.org/10.1016/j.jallcom.2012.12.033

[19] X.P. Ji, W.C. Cao, C.Z. Bu, K. He, Y.D. Wu, G.H. Zhang, A new route for preparing Mo-10 wt% Cu composite compacts, Int. J. Refract. Met. H., 81 (2019) 196-205

[20] D. Jelić, B. Tomić-Tucaković, S. Mentus, A kinetic study of copper(II) oxide powder reduction with hydrogen, based on thermogravimetry, Thermochim. Acta 521 ( 2011) 211-217, doi:10.1016/j.tca.2011.04.026.

[21] J. Li, J.W. Mayer, K.N. Tu, Nucleation and growth of $Cu_2O$ in the reduction of CuO thin films, Phys. Rev. B 45 (1992) 5683-5686, doi: 10.1103/physrevb.45.5683

[22] J. Y. Kim, J. C. Hanson, A.I. Frenkel, P.L. Lee, Reaction of CuO with hydrogen studied by using synchrotron-based x-ray diffraction, J. Phys.: Condens. Matter 16 (2004) 3479-3484, doi:10.1088/0953-8984/16/33/008

[23] M. S. W. Vong, P. A. Sermon, K. Grant, In-sity study of reduction of copper catalyst, Catal. Lett. 4 ( 1990) 15-24, doi:10.1007/BF00764866

[24] J.Y. Kim, J.A. Rodriguez, J.C. Hanson, A.I. Frenkel., P.L. Lee, Reduction of CuO and $Cu_2O$ with $H_2$: H embedding and kinetic effects in the formation of suboxides, J. Am. Chem. Soc. 125 (2003) 10684-10692, doi:10.1021/ja0301673

[25] J.A. Rodriguez, J.Y. Kim, J.C. Hanson, M. Pérez and A.I. Frenkel, Reduction of CuO in $H_2$: in situ time-resolved XRD studies, Catal. Let. 85 (2003) 247-254, doi:10.1023/A:1022110200942.

[26] T. Ressler, J. Wienhold, R.E. Jentoft, Formation of bronzes during temperature-programmed reduction of $MoO_3$ with hydrogen—an in situ XRD and XAFS study, Solid State Ionics, 141-142 (2001) 243-251, https://doi.org/10.1016/S0167-2738(01)00747-0.

[27] W.V. Schulmeyer, H.M. Ortner, Mechanisms of the hydrogen reduction of molybdenum oxides, Int. J. Refract. Met. H. 20 (2002) 261-269, https://doi.org/10.1016/S0263-4368(02)00029-X.

[28] J. Sloczynski, W. Bobinski, Autocatalytical effect in the process of metal oxide reduction. II Kinetics of Molybdenum oxide reduction, J. Solid State Chem. 92 (1991) 436 – 448. https://doi.org/10.1016/0022-4596(91)90350-Q.

[29] S. Majumdar, L.G. Sharma, I. Samajdar, P. Bhargava, Kinetic study on hydrogen reduction of $MoO_3$ and morphological analysis of reduced Mo powder, Metall. Mater. Trans. B, 39B (2008) 431- 438. doi:10.1007/s11663-008-9152-8.

[30] M. Saghafi, S. Heshmati-Manesh, A. Ataie, A.A. Khodadadi, Synthesis of nanocrystalline molybdenum by hydrogen reduction of mechanically activated $MoO_3$ Int. J. Refract. Met. H. 30 (2012) 128-132, doi:10.1016/j.ijrmhm.2011.07.014

[31] G.-S. Kim, Y. J. Lee, D.-G. Kim, Y.D. Kim, Consolidation behavior of Mo powder fabricated from milled Mo oxide by hydrogen-reduction, J. Alloys Compd. 454 (2008) 327-330, DOI10.1016/j.jallcom.2006.12.039

[32] J. Dang, G.H. Zhang, K.C. Chou, F.G. Reddy, Y. He, Y. Sun, Kinetics and mechanism of hydrogen reduction of $MoO_3$ to $MoO_2$ Int. J. Refract. Met. H. 41 (2013) 216-223, https://doi.org/10.1016/j.ijrmhm.2013.04.002.

[33]. L.Wang, Z.-L. Xue, A. Huang, J.-T. Wang, Mechanism and kinetics of reducing $MoO_3$ to $MoO_2$ with CO-15vol% $CO_2$ mixed gases, ACS Omega 4 (2019) 20036-20047, DOI: 10.1021/acsomega.9b03171

[34] J. Dang, G.-H. Zhang, K.-C. Chou, Study on Kinetics of Hydrogen Reduction of $MoO_2$, Int. J. Refrac. Met. H. 41 (2013) 356-362, doi: 10.1016/j.ijrmhm.2013.05.009

[35] B.-S. Kim, E.-Y. Kim, H.-S. Jeon, H.-I. Lee, J.-C. Lee, Study on the Reduction of Molybdenum Dioxide by Hydrogen, Mater. Trans., 49 (2008) 2147-2152, DOI: 10.2320/matertrans.MER2008103

[36] S.Mentus, B. Tomić-Tucaković, D. Majstorović, R. Dimitrijević, Gel-combustion synthesis of NiO–$MoO_3$ mixtures and their reduction to Ni–Mo alloys, Mater. Chem. Phys., 12 (2008) 254–261, doi:10.1016/j.matchemphys.2008.05.043

[37] S.Mentus, Gel Combustion Synthesis, in M.Lackner Ed., Combustion Synthesis, Bentham Science Publ. (2010) Ch. 5, p. 55-71 (eISBN: 978-1-60805-155-7). https://doi.org/10.2174/978160805155711001010055.

[38] E. A. Gulbransen, K. F. Andrew, and F. A. Brassart, Oxidation of Molybdenum 550 $^{o}$ to 1700 $^{o}$C, J. Electrochem. Soc., 110 (1963) 952 - 959 https://citeseerx.ist.psu.edu/viewdoc/download?doi=10.1.1.854.8433&rep=rep1&type=pdf

[39] G.R. Smolik, D.A. Petti, S.T. Schuetz, Oxidation, volatilization and redistribution of molybdenum from TZM alloy in air, Idaho National Engineering and Environmental Laboratory, INEEL/EXT-99-01353 (2000), https://digital.library.unt.edu/ark:/67531/metadc888418/m2/1/high_res_d/911479.pdf

[40] L. Álvarez-Falcón, F. Viñes, A. Notario Estévez, F. Illas, On the hydrogen adsorption and dissociation on Cu surfaces and nanoparticles, Surf. Sci., 646 (2016) 221-229, doi:10.1016/j.susc.2015.08.005.

[41] H.A. Michelsen, C.T Rettner, D.J. Auerbach, The Adsorption of Hydrogen at Copper Surfaces: A Model System for the Study of Activated Adsorption. In: Madix R.J. (eds) Surface Reactions. Springer Series in Surface Sciences, Vol. 34. (1994) Springer, Berlin, Heidelberg. doi:10.1007/978-3-642-78746-1_6

[42] G. Feng, M.V. Ganduglia-Pirovano, C.F. Huo, J. Sauer, Hydrogen Spillover to Copper Clusters on Hydroxylated gamma-Al2O3, J. Phys. Chem. C. 122 (2018) 1932-7447. DOI: 10.1021/acs.jpcc.8b03764.

[43] CRC Handbook of Chemistry and Physics 84th Edition, D.R.Lide Ed., CRC Press LLC 2003-2004, https://doi.org/10.1021/ja0336372

[44] A.A. Levchenko, T. Basalik, P. Le Parlouer, A. Navrotsky, High-temperature calorimetry and thermal analysis of perovskites, 34th International Conference and Exposition on Advanced ceramics and Composites, Daytona Beach Fl USA Jan 24-29, 2010, Poster ICACC-S6-P030-201, https://seltokphotonics.com/upload/iblock/fa4/fa4d1155eb267e11670d87aef7dc9833.pdf

[45] Yu-ying Zhang, Meng-jie Wang, Chun-ran Chang, Kang-zhen Xu, Hai-xia Ma, Feng-qi Zhao, A DFT study on the enthalpies of thermite reactions and enthalpies of formation of metal composite oxide, Chemical Physics 507 (2018) 19-27, doi:10.1016/j.chemphys.2018.04.004

[46] J.L. Brito, J. Laine, Reducibility of Ni-Mo/Al2O3 Catalysts: A TPR Study J. Catal. 139 (1993) 540-550, doi:10.1006/jcat.1993.1047 ]

[47] A.K. Burnham, L.N. Dinh, A comparison of isoconversional and model-fitting approaches to kinetic parameter estimation and application predictions, J. Therm. Anal. Calorim. 89 (2007) 479 – 490, https://doi.org/10.1007/s10973-006-8486-1.

[48] Kinetics software KINETICS2015 geoisochem.com/software/kinetics2015/index.html

[49] S. Vyazovkin, W. Linert, Thermally induced reactions of solids:Isokinetic relationships of non-isothermal systems, Int. Rev. Phys. Chem., 14 (1995) 355-369Doi.10.1080/01442359509353314

[50] A.Khawam, D.R.Flanagan, Solid-state kinetic models: Basics and mathematical fundamentals, J. Phys. Chem. B, 110 (2006) 17315- 17328. https://doi.org/10.1021/jp062746a.

[51] R. L. Braun and A. K. Burnham, Global Kinetic Analysis of Complex Materials, Energ. Fuel., 13 (1999)1-22. https://doi.org/10.1021/ef9800765.

[52] A.K. Burnham, R.L. Braun, An appropriate kinetic model for well-preserved algal kerogens, Energ. Fuel. 10 (1996) 49-59, DOI: 10.1021/ef950142s

[53] H. H. Kung, Transition Metal Oxides, Surface Chemistry and Catalysis, Elsevier Sci.Publ. 1989, p 91-109. ISBN: 0 444 87394 5

[54] H.J. Flynn, L.A. Wall, General Treatment of the Thermogravimetry of Polymers, J. Res. Natl. Bur. Stand. A, Phys. Chem. 70 (1966) 487–523, http://dx.doi.org/10.6028/jres.070A.043

[55] T. Ozawa. A new method of analyzing thermogravimetric data, Bull. Chem. Soc. Jpn. 38 (1965) 1881–1886, doi:10.1246/bcsj.38.1881

[56] H.E. Kissinger, Reaction Kinetics in Differential Thermal Analysis, Anal. Chem. 29 (1957) 1702-1706, doi:10.1021/ac60131a045

[57] C.R. Li, T.B. Tang, Dynamic thermal analysis of solid state reaction, The ultimate method for data analysis?, J. Therm. Anal. Calorim. 49 (1997) 1243-1248.

doi:10.1007/bf01983680

[58] A. Samsuri, F. Salleh, S.Tengku, R. Chaman, A. Yarmo, Study on the Reduction Behaviour of Nickel Doped Molybdenum Trioxide by Using Carbon Monoxide as Reductant. Int. J.Chem. Eng. Appl. 7 (2016) 16-21, DOI: 10.7763/IJCEA.2016.V7.534.

Figure captions

Fig. 1 XRD diagrams of $CuO$-$MoO_3$ samples, for different molar fractions ( x) of CuO. The labels of diffraction lines: o-CuO, + - $Cu_3Mo_2O_9$, □- α-$CuMoO_4$, x - $MoO_3$

Fig 2. The SEM pictures of $xCuO$-$(1-x)MoO_3$ system. x (from top downwards) = 0.9; 0.7; 0.5; 0.3 and 0.1. The length of white bar is 0.1μm

Figure 3. The TG curves of reduction of $xCuO$:$(1-x)MoO_3$ samples in Ar + 25% $H_2$ flow, recorded at a common heating rate of 10 °C $min^{-1}$

Fig 4. The TG diagrams of selected $xCuO$-$(1-x)MoO_3$ compositions, with their first order derivatives. Left: CuO-rich region, right: $MoO_3$-rich region of compositions

Fig 5. The TG curves of reduction of $0.5CuO$-$0.5MoO_3$ system at various heating rates

Figure 6. The dependence of preexponential factor A (empty squares) and energy of activation E (full circles) on the fraction reacted, obtained by expanded Friedman isoconversional method, for low-temperature (left) and high-temperature (right) region of reduction of $0.5CuO$-$0.5\ MoO_3$ oxide system

Figure 7. Experimental (symbols) and simulated (solid lines) dependence of conversion degree on temperature for low-temperature (left) and high-temperature (right) reastion regions of 0.5CuO-0.5 $MoO_3$ oxide mixture: the heating rates (from left toward right) 5, 7.5 , 15 and 25 °C $min^{-1}$

Fig 8. X-ray diffractogramms of Cu-Mo composites. The Mo lines are labeled by crosses and Cu lines by circles

Fig 9. The SEM pictures of xCu-(1-x)Mo composites: X (from top downwards) = 0.9, 0.7, 0.5, 0.3 and 0.1. The length of white bar is 1 μm

Table captions

Table I. The mass loss, (%) for reduction of CuO, and first-step reduction of $MoO_3$ ( f.s), their sum calculated and determined experimentally, and actual mass upon complete reduction, calculated ($m_{tot}$, %) and experimentally determined ($m_{tot}$, % exp.)

Author Statement

D.Jelić synthesized the samples and committed the thermogravimetric measurements. S. Zeljković performed kinetic analysis. D. Jugović performed XRD measurements and XRD data analysis. S.Mentus conteptualized the study, provided SEM observations and wrote original draft.

$$\alpha = \frac{m_0 - m_t}{m_0 - m_f} \quad (1)$$

$$\ln\left(\frac{d\alpha}{dt_\alpha}\right) = -\frac{E_\alpha}{RT_\alpha} + \ln\{A_\alpha\, f(\alpha)\} \quad (2)$$

$$\frac{d\alpha}{dt} = k(1-\alpha)^n(1-q(1-\alpha))^m \quad (3)$$

$$\ln(\beta) = \ln\left[A\frac{f(\alpha)}{(d\alpha/dT)}\right] - \frac{E_\alpha}{RT} \quad (4)$$

$$\ln\frac{\beta}{T_{\max}^2} = \ln\frac{AR}{E_\alpha} - \frac{E_\alpha}{RT_{\max}} \quad (5)$$

Table I. The mass loss, (%) for reduction of CuO , and first-step reduction of $MoO_3$ ( f.s), their sum calculated and determined experimentally , and actual mass upon complete reduction, calculated ($m_{tot}$, %) and experimentally determined ($m_{tot}$, % exp.)

| xCuO | $\Delta m_{CuO}$, % calc. | $\Delta m_{MoO3}$(f.s.),% calc. | $\Delta m_{CuO}+\Delta m_{MoO3}$(f.s.), % calc. | $\Delta m_{CuO}+\Delta m_{MoO3}$(f.s.), % exp. | $m_{tot}$, % calc | $m_{tot}$, % exp. |
|---|---|---|---|---|---|---|
| 1.0 | 20.1 | 0.00 | 20.1 | 20.0 | 79.90 | 80.0 |
| 0.9 | 18.1 | 1.11 | 19.2 | 18.5 | 78.57 | 78.2 |
| 0.8 | 16.09 | 2.22 | 18.3 | 16.1 | 77.24 | 77.1 |
| 0.7 | 14.08 | 3.33 | 17.4 | 15.0 | 75.92 | 76.8 |
| 0.6 | 12.07 | 4.44 | 16.5 | 14.0 | 74.59 | 74.5 |
| 0.5 | 10.06 | 5.55 | 15.6 | 12.5 | 73.27 | 73.4 |
| 0.4 | 8.045 | 6.66 | 14.7 | 13.0 | 71.96 | 71.9 |
| 0.3 | 6.03 | 7.77 | 13.8 | 12.0 | 70.67 | 70.6 |
| 0.2 | 4.02 | 8.88 | 12.9 | 11.5 | 69.31 | 68.7 |
| 0.1 | 2.01 | 9.99 | 12.0 | 10.8 | 67.99 | 67.8 |
| 0.0 | 0.00 | 11.1 | 11.1 | 11.2 | 66.7 | 66.6 |

Highlights

Reduction of $CuO$-$MoO_3$ system by hydrogen was investigated thermogravimetrically

Low-temperature and high-temperature reduction regions are clearly separated

Metallic Cu accelerates reduction of both $MoO_3$ and $MoO_2$

Kinetic parameters of equimolar mixture reduction determined by isoconversional method

Homogeneity of Cu-Mo composite is better at lower Cu fractions

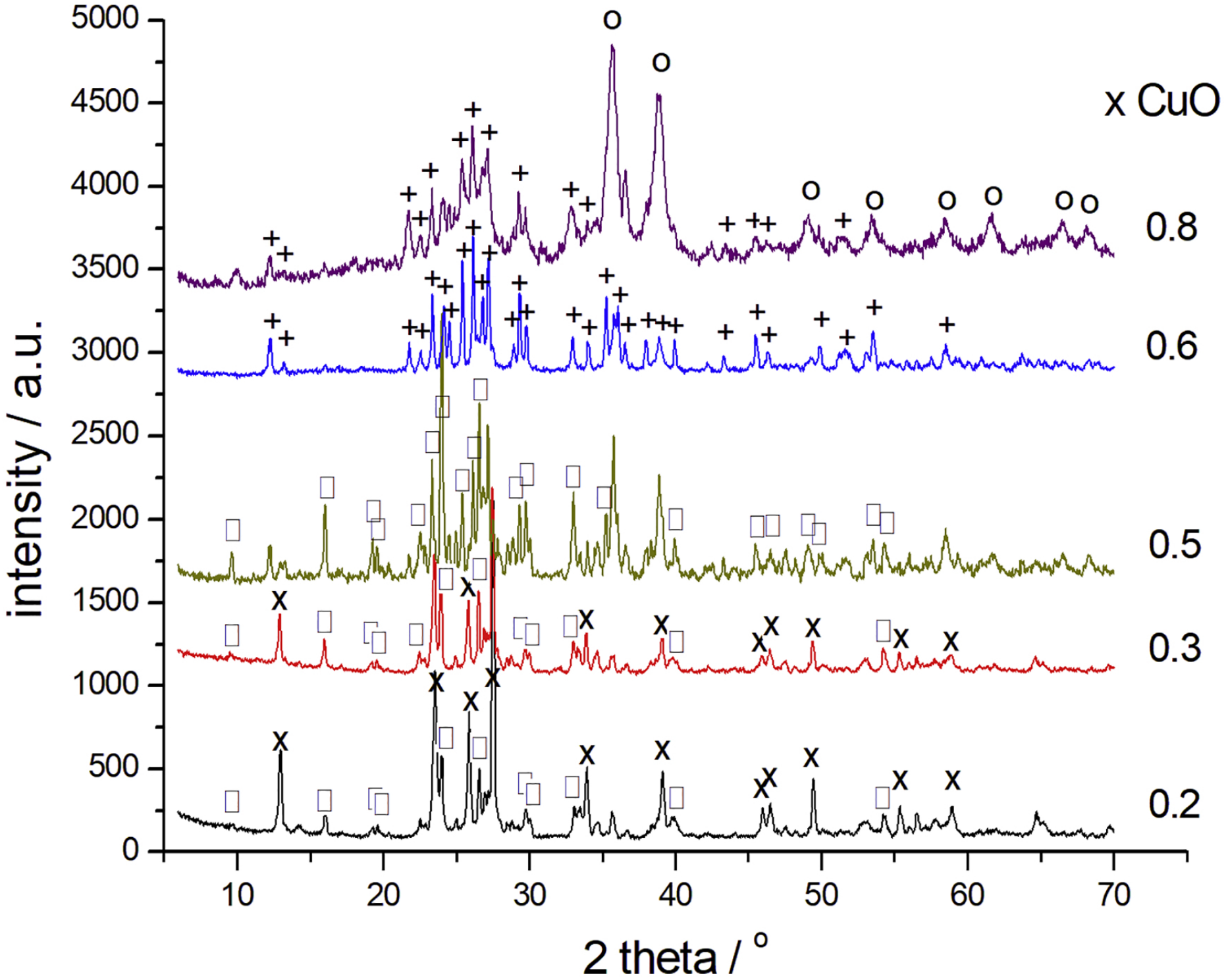
x CuO
0.8
0.6
0.5
0.3
0.2
intensity / a.u.
2 theta / °
5000
4500
4000
3500
3000
2500
2000
1500
1000
500
0
10
20
30
40
50
60
70

Figure 1

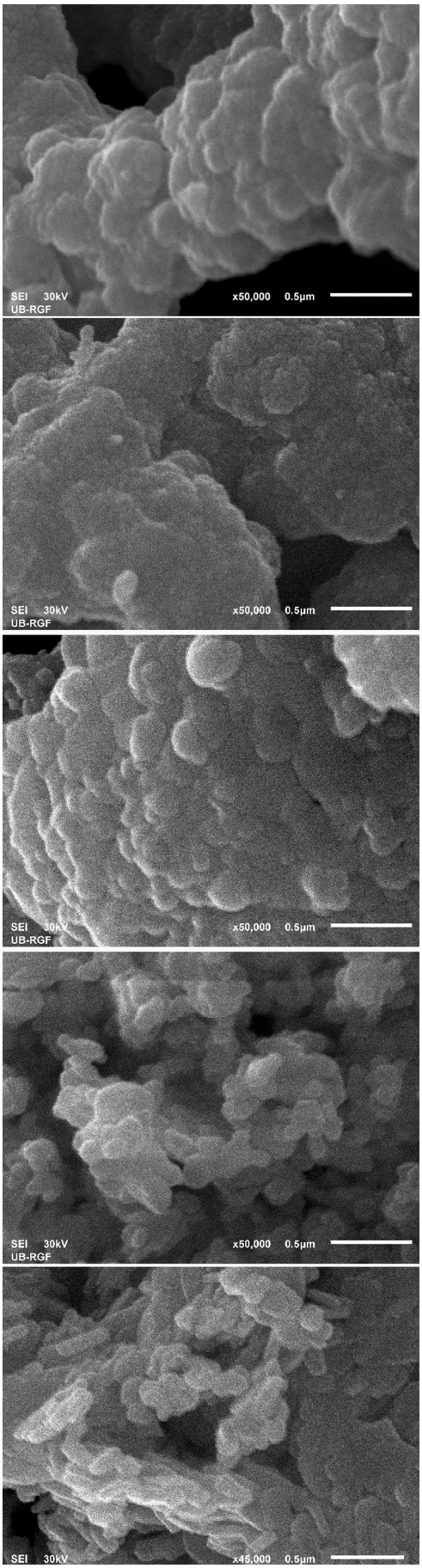
SEI 30kV
UB-RGF
x50,000 0.5µm
SEI 30kV
UB-RGF
x50,000 0.5µm
SEI 30kV
UB-RGF
x50,000 0.5µm
SEI 30kV
UB-RGF
x50,000 0.5µm
SEI 30kV
x45,000 0.5µm

Figure 2

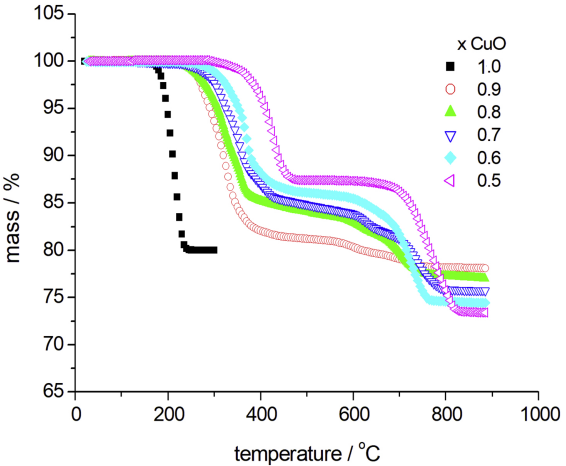
x CuO
1.0
0.9
0.8
0.7
0.6
0.5
mass / %
temperature / °C

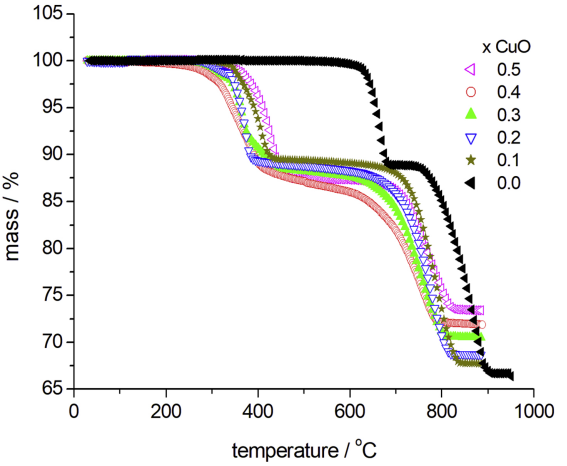
x CuO
0.5
0.4
0.3
0.2
0.1
0.0
mass / %
temperature / °C

Figure 3

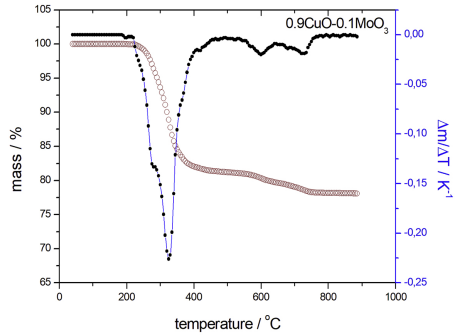
0.9CuO-0.1MoO3
mass / %
Δm/ΔT / K-1
temperature / °C

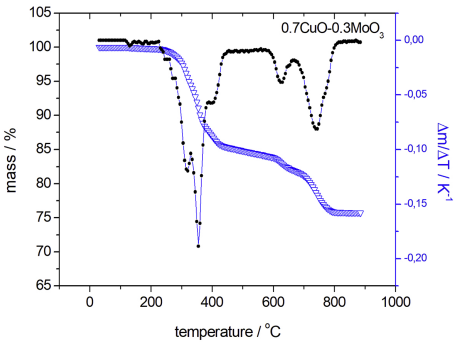
0.7CuO-0.3MoO3
mass / %
Δm/ΔT / K-1
temperature / °C

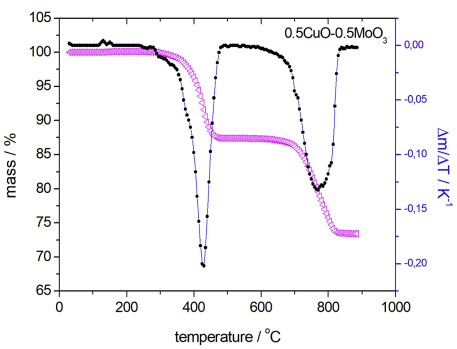
0.5CuO-0.5MoO3
mass / %
Δm/ΔT / K-1
temperature / °C

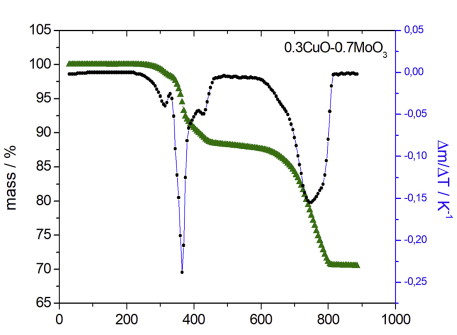
0.3CuO-0.7MoO3
mass / %
Δm/ΔT / K-1
temperature / °C

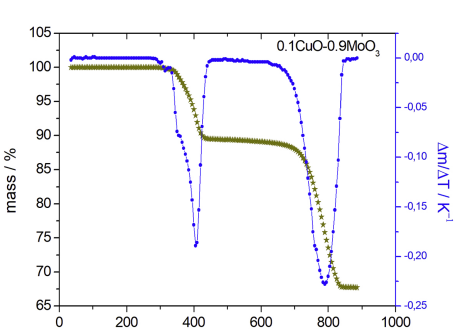
0.1CuO-0.9MoO3
mass / %
Δm/ΔT / K-1
temperature / °C

Figure 4

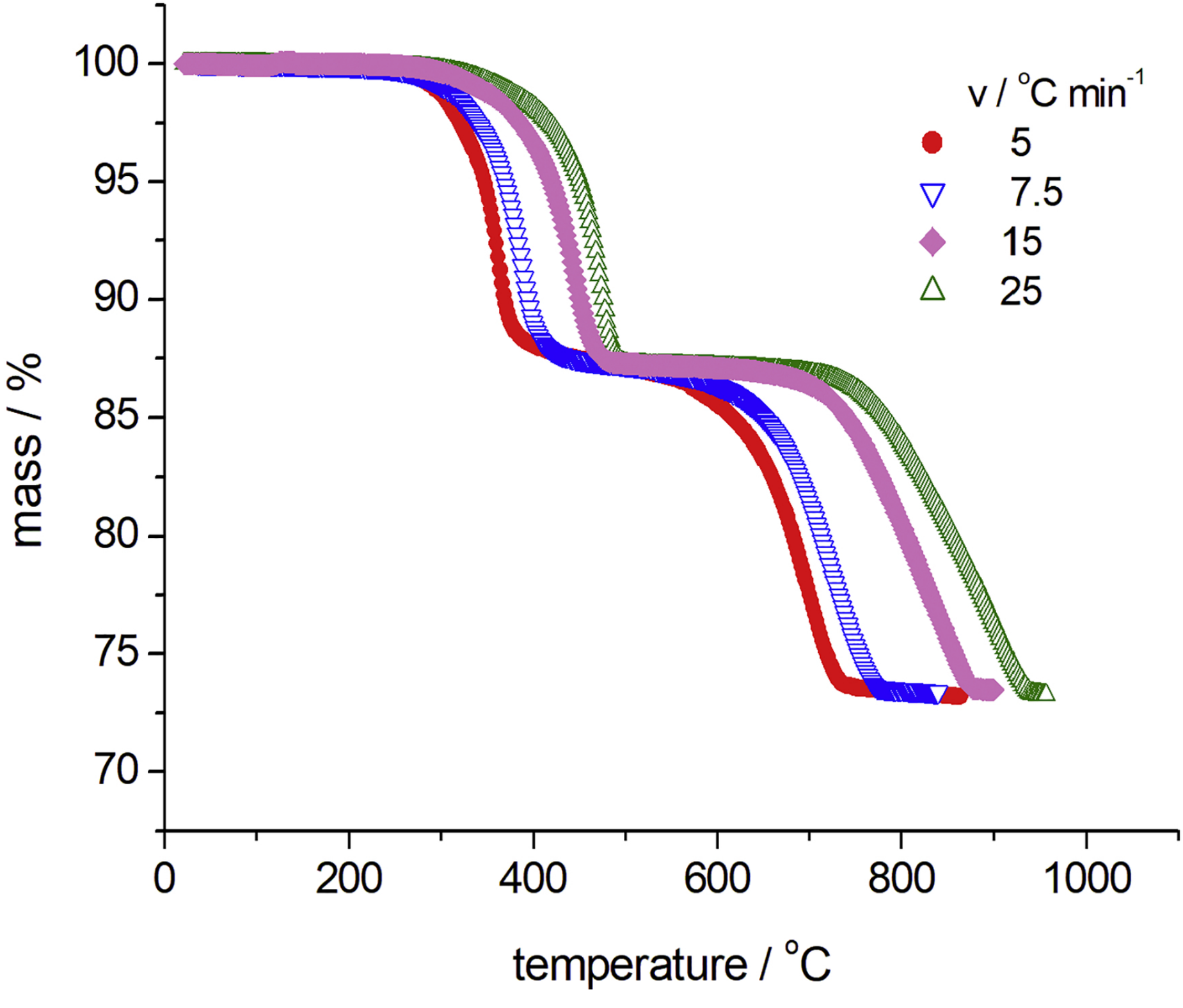
100
95
90
85
80
75
70
mass / %
0
200
400
600
800
1000
temperature / °C
v / °C min-1
5
7.5
15
25

Figure 5

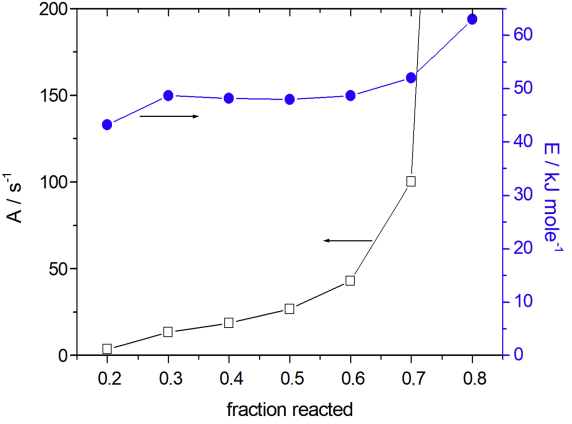
A / s-1
E / kJ mole-1
fraction reacted
200
150
100
50
0
60
50
40
30
20
10
0
0.2
0.3
0.4
0.5
0.6
0.7
0.8

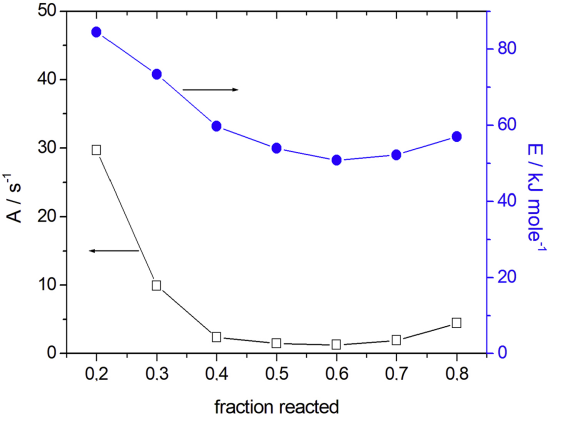
A / s-1
E / kJ mole-1
fraction reacted
50
40
30
20
10
0
80
60
40
20
0
0.2
0.3
0.4
0.5
0.6
0.7
0.8

Figure 6

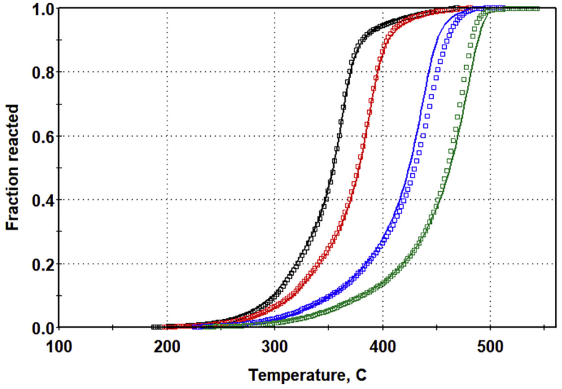
Fraction reacted
1.0
0.8
0.6
0.4
0.2
0.0
100
200
300
400
500
Temperature, C

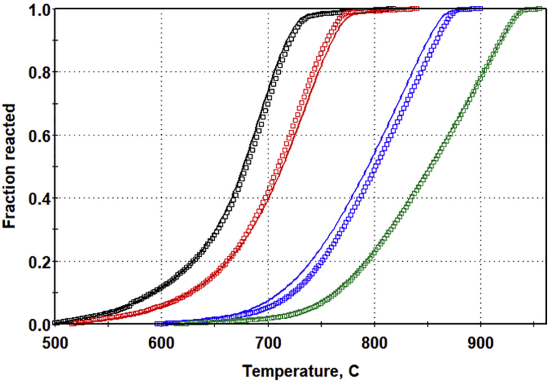
Fraction reacted
1.0
0.8
0.6
0.4
0.2
0.0
500
600
700
800
900
Temperature, C

Figure 7

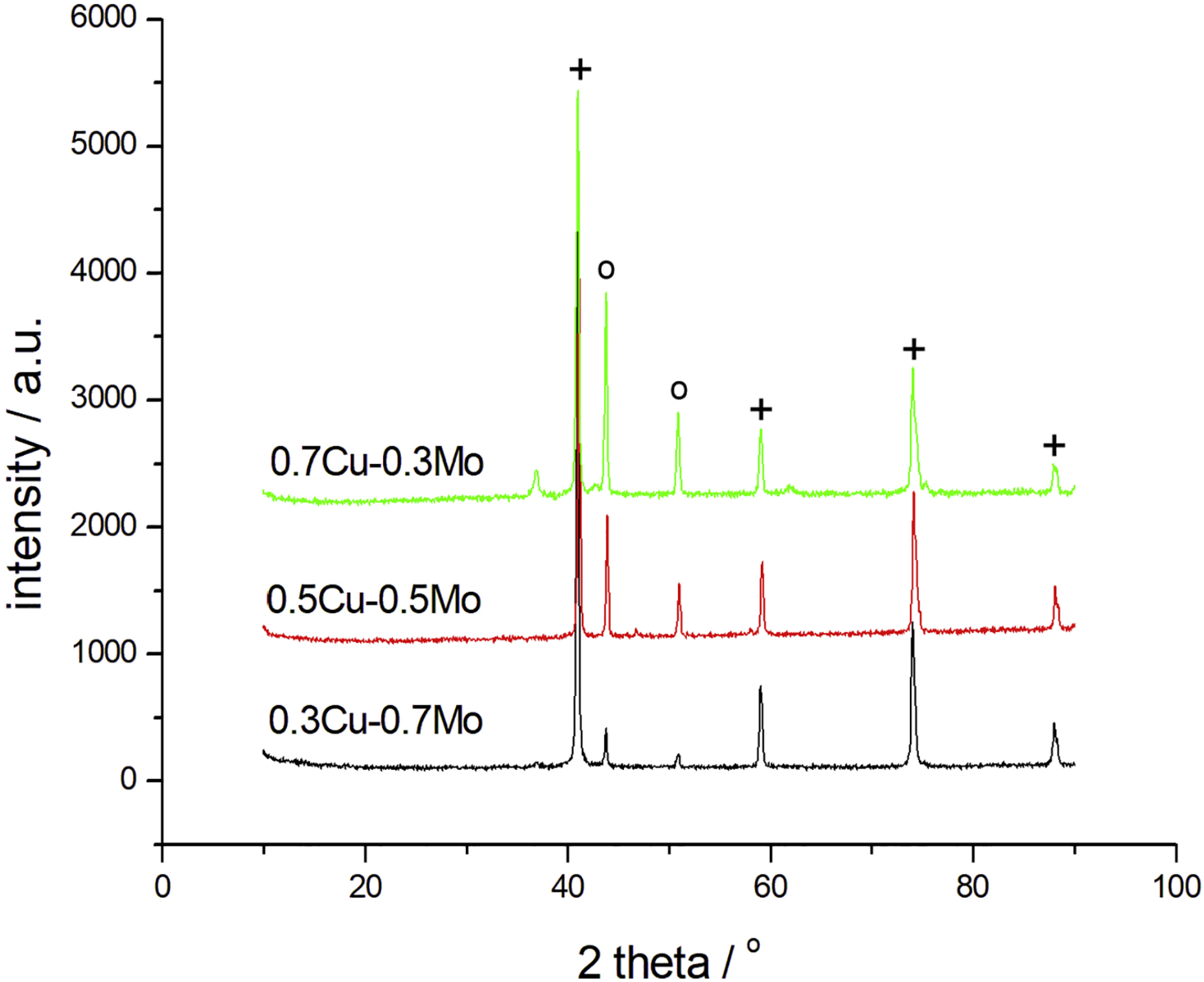
6000
5000
4000
3000
2000
1000
0
intensity / a.u.
0
20
40
60
80
100
2 theta / °
0.7Cu-0.3Mo
0.5Cu-0.5Mo
0.3Cu-0.7Mo
+
o
o
+
+
+

Figure 8

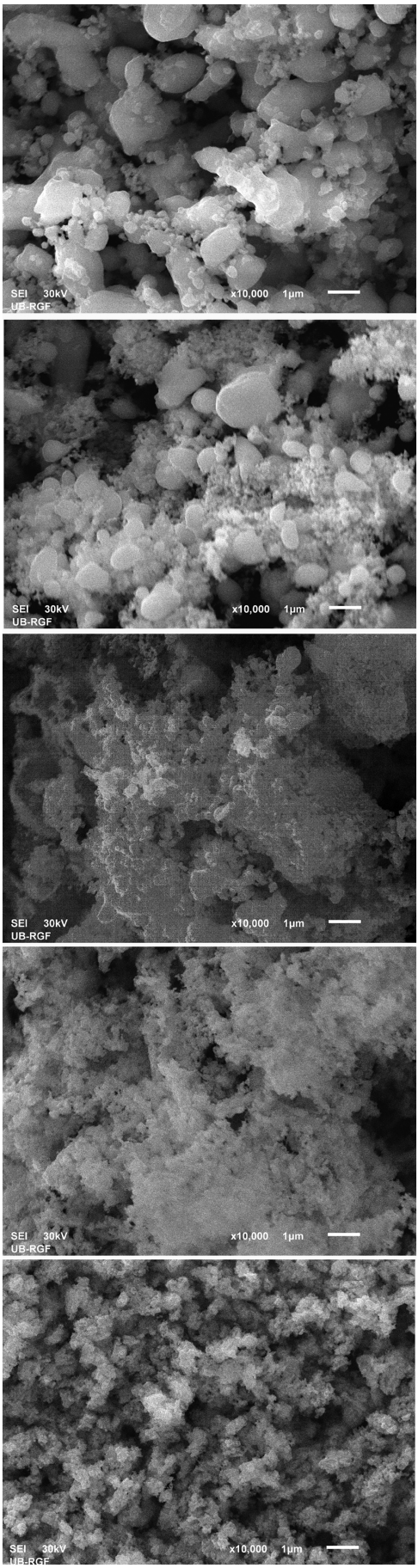
SEI 30kV
UB-RGF
x10,000 1μm
SEI 30kV
UB-RGF
x10,000 1μm
SEI 30kV
UB-RGF
x10,000 1μm
SEI 30kV
UB-RGF
x10,000 1μm
SEI 30kV
UB-RGF
x10,000 1μm

Figure 9